DEVELOPMENT OF A MULTI-LAYERED MAP MANAGEMENT SYSTEM UTILIZING THE NONHOMOGENEOUS MARKOV CHAIN APPROACH

By

TAKAO OKUI

A DISSERTATION PRESENTED TO THE GRADUATE SCHOOL
OF THE UNIVERSITY OF FLORIDA IN PARTIAL FULFILLMENT
OF THE REQUIREMENTS FOR THE DEGREE OF
DOCTOR OF PHILOSOPHY

UNIVERSITY OF FLORIDA

1999

ACKNOWLEDGMENTS

The author would like to express his gratitude to the member of his supervisory committee, Dr. Carl Crane, Dr. Joseph Duffy, Dr. Paul Mason, Dr. John Ziegert, and Dr. Murali Rao, for their guidance. Special thanks go to Dr. Crane who brought the author on board this project and has provided advice for graphic simulation programs, and to Dr. Rao who has provided invaluable advice from the viewpoint of mathematics.

This work would have not been possible without the invaluable support of the author's friends in order to live in a foreign country alone for more than three years without going back to his home country. Thanks go to Dean Hutchinson, Paul Johnston, Craig Walker, Robert and Kathleen McGee, Laura and Brian Gill, David Novick, Robin Wilson, Arturo Rankin, Van and Carol Chesney, Steve Kowkabany, Tony Shawver, Peter Tandon, Sadie Greenberg, Phil Adsit and Waheed Abbasi for their moral support.

Finally, special thanks go to the author's parents; Kennichi and Eiko Okui and to the author's friends in his home country; Tsutsui Fuyuko, Harumi Konno, and Masaomi Takeuchi who have provided the moral support.

TABLE OF CONTENTS

Abstract of Dissertation Presented to the Graduate School
of the University of Florida in Partial Fulfillment of the
Requirements for the Degree of Doctor of Philosophy

DEVELOPMENT OF A MULTI-LAYERED MAP MANAGEMENT SYSTEM
UTILIZING THE NONHOMOGENEOUS MARKOV CHAIN APPROACH

By

Takao Okui

May 1999

Chairman: Dr. Carl D. Crane III
Major Department: Mechanical Engineering

Map building is one of the most important technologies for a variety of robotic vehicles. Obstacle information around a vehicle will be used for obstacle avoidance and global obstacle information will be used for path planning and exploration. Especially, when a vehicle moves in a hazardous area, map information becomes tremendously crucial.

This doctoral research deals with map management for a large-scale outdoor environment where data are obtained from a moving vehicle. A multi-layered map management system is developed that consists of local grid map and a global contour map.

The local grid map is represented as a grid model and the management system is based on a concept of *uncertainty*. *Uncertainty* can be classified under one of three categories: randomness, fuzziness, and indeterminacy. From the viewpoint of *uncertainty*,

previous grid model techniques are discussed. The fuzzy model approach for range sensors and a new update formula utilizing a nonhomogeneous Markov chain are then presented.

The global contour map is represented as a boundary representation. The larger the area in which a vehicle moves, the more data that are generated. To reduce the size of data required to be stored on the on-board computer, conversions between the grid model and boundary representation are developed. A cell in a grid model is regarded as a bubble and like a bubble becomes bigger when two bubbles are fused. Polygonal contours of probability are thus produced as a vehicle moves. Similarly, a cell in the grid model is initialized using the polygonal contour when the vehicle returns to a previously visited location. This strategy is introduced in detail and is demonstrated in simulation.

CHAPTER 1
INTRODUCTION

As seen in the Mars exploration mission by NASA's Jet Propulsion Laboratory using a rover robot named Sojourner, one of the most important issues in the area of unmanned mobile robots is the ability to perceive the robot's surroundings with a minimum of a priori information for the accomplishment of its goal. Robots in this environment must move over extensive natural terrain which mainly consists of scattered rocks on the ground and ditches. It is necessary to combine views obtained from many different locations into a single consistent map so that high level task planning can occur.

To implement a map, it is inevitable that the robot uses information about the environment that is provided by its sensors. These sensor data represent the obstacles implicitly or explicitly. Visual sensing has enormous potential for providing information about the environment. However, image processing is computationally very expensive under the constraint of real-time operation. Many robot systems use range images acquired from active ranging sensors or passive stereo vision. For example, ultrasonic sensors have been used extensively for obstacle detection on mobile robots. These sensors have a conical field of view and return a radical measure of the distance to the nearest object within the cone. They are able to get distances directly through simple signal processing with little power consumption, are remarkably simple to use, are compact, and are low cost.

Each sensor has limitations, however, such as resolution, field of view, sampling time, measurement accuracy, and dynamic range. Further, sensor measurements are contaminated by noise, and spurious measurements are caused by the physical operating conditions.

For instance, ultrasonic sensors have three major shortcomings. One is poor angular resolution that limits the accuracy in determining an edge of an object. Second, frequent misreading is caused by either ultrasonic noise from external sources such as another robot's ultrasonic sensors or stray signal or reflections from neighboring sensors known as crosstalk. Third are specular reflections which occur when the angle between the acoustic axis and the normal to a smooth surface is too large. Stereo vision also has uncertainty in measurement caused by imperfectly known pixel positions and calibration parameters such as focal length and extrinsic parameters such as relative position and orientation of the cameras.

To reduce or compensate these sources of noise, there are primarily three techniques. One is the conventional technique of using a low pass filter, fast Fourier transform, or averaging. Most noise is high frequency, so the high frequencies are filtered without losing necessary information.

Second is the fusion technique. This also deals with only one sampling datum or a small set of previous sampling data, but it uses the data from more than one of the same type of sensors or from different types of sensors. Multiple sensors can perceive the environment with better accuracy and a wider sensing field than if one sensor were used alone. For instance, the combination of ultrasonic sensors and stereo vision has an

advantage due to a complementary error characteristic concerning range and angular resolution of the sensors.

Third is the map technique. This deals with data collected over time from one or more sensor. A map typically starts with a priori information. It is updated by explicitly comparing features from current sensor data with features from the given map or updated map over time. The way in which the map is organized and represented has a major impact on the efficiency with which the robot can carry out its tasks. The author has found that the bulk of literature related to the map technique can be classified under one of five categories from the view point of map representations: topological graph, boundary representation, feature-based model, grid model, and multi-layered representation by combining some of the representations.

Topological graphs are expressed using higher level abstraction such as nodes and connections. The environment is a graph consisting of nodes and edges, where the robot can navigate from one node to another through an edge connecting these two nodes. Topological graphs are used for global path planning in large-scale spaces because less information is required which reduces the required computational resources. However, complex calculations will be necessary to obtain higher abstracted data, and updating of the topological graph in a dynamic environment is complicated.

Boundary representations are polygons for two dimensions and polyhedral for three dimensions to express an approximate boundary of an object. Polygons are expressed using a linked list of vertices. Usually, polygonal obstacles are used in global path planning to produce the visibility graph, Voronoi diagram, tangent graph, Delaunay

triangulation, potential field and so on. However it is very difficult to deal with the uncertainty in sensor measurement.

A feature-based model is represented by intrinsic geometrical information such as center of mass, matrix of inertia, maximum of elevation, and total area. But updating a feature-based representation becomes much more complex when the robot moves while acquiring sensor data.

Grid models are two dimensional or three dimensional tessellations of space into congruent square cells where each cell contains some value indicating the measure of confidence that an obstacle exists within the cell area. Usually the greater the value in a cell, the greater the level of confidence that the cell is occupied by an obstacle. If no information is available, a cell is considered unknown. A new sensor reading introduces new information that is combined with the current value stored in a cell to give a new value. This can accommodate information from different sensors supplying qualitatively different range information and cope with sensor error and represent uncertainty arising from sensor noise over time because misreading occurs at random and therefore produces mostly isolated cells with low values. Obviously, to enhance the map accuracy of existence of an obstacle, it is necessary that the same cell and its neighboring cells must be repeatedly detected, by which the robot moves slowly or remains stationary during the sensing process instead. Moreover, when applied to large spaces such as when operating outdoors, this representation becomes computationally expensive.

The concept of multi-layered representations has the benefit of being able to choose the most appropriate representation for the accomplishment of each task. However it is very difficult to implement a multi-layered representation with updates as the robot

moves due to processor limitations. Also there is the problem in maintaining consistency between the representations, as real-time map conversion algorithms are needed. Recently, with processor speed increasing and with the availability of parallel bus architectures, maintaining multiple representation in real-time systems is becoming more feasible.

In this research, the problem of constructing and maintaining a map is treated with the development of a map management system. The maintenance and update of a map for obstacle avoidance, path planning, and exploration are the primary motivation. Updating the map is complex and difficult due to noisy sensor data, limited resources installed on a vehicle, and limited observation time as the vehicle moves in an outdoor environment while acquiring sensor data, which is necessary for real-time navigation.

The proposed map management system was developed by using a multi-layered map, i.e. a local grid map and a global contour map. A grid model is used as a local map to fuse data from different sensors over time for obstacle detection with a consideration of measurement uncertainties. A boundary representation is used in a global map to solve the memory storage problem that would exist if a grid model alone was used to model a large-scale environment. The representation produces a polygon approximation of obstacle boundaries and free space boundaries. The system maintains a consistency between the two map representations by obstacle addition, deletion, and modification, and produces a local map around the current robot's position for obstacle avoidance and a global map for path planning and exploration. The concept of the map management system is shown Figure 1-1.

A survey of relevant earlier map management methods is presented in chapter 2, while chapter 3 introduces the map management system and defines the objective and the assumptions used in this research. It also states the contribution of this work to the area of study. Chapter 4 discusses previous works of update methods for a grid map with sensor modeling used in the management system. Chapter 5 details the proposed update method for a local grid map by utilizing the nonhomogeneous Markov chain approach with fuzzy modeling of range sensors. The real-time conversion algorithm between grid model and boundary representation is described in chapter 6. Chapter 7 presents the results of the simulation, and conclusions are presented based on these results.

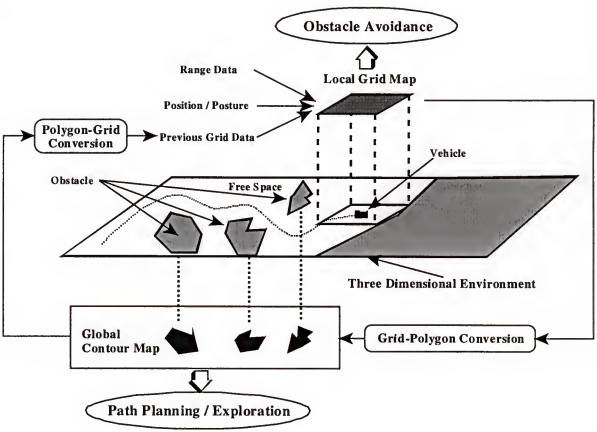

Figure 1-1 Concept of Map Management System

CHAPTER 2
LITERATURE REVIEW

A map management system must typically deal with range data from a variety of sensors such as ultrasonic, stereo vision, and laser scanner sensors. These sensors have their own uncertainties in measurement and are contaminated by noise. The system must fuse these acquired data into one uniform data structure and transform the data into a map. The map specifies the geometric layout of a navigable space, the location of objects of interest, and the robot's own location. As a robot moves in an outdoor terrain it also must update a map according to changes in the environment. Therefore, the representation is one of the most important issues for the map management system. Many references demonstrate map building and usage; however, there are no references dealing with the map management itself. The majority of recent work using a map is in the area of navigation, localization and path planning. The author has found that the literature can be classified under one of five categories: grid model, boundary representation, feature-based model, topological graph, and multi-layered representation.

Grid Model

Recent development of map representations for navigation mainly uses a grid model. Moravec and Elfes[Elf87b, Mor85, Mor88] introduced the grid model for a map representation called occupancy grids. In this grid model, the robot work area is represented by a two dimensional array of square elements denoted as cells. Each cell

contains a certainty value that indicates the probabilistic estimate of its occupancy by an object in the environment. Cell values are updated by a Bayesian estimation model that takes into account the characteristics of a given sensor. A new sensor reading introduces new information in the form of the conditional probability. This function is combined with the current probability estimates stored in a cell to give a new estimate. The final map has cell values; for example, in the range (0.0, 1.0), where values less than 0.5 represent probability of empty region, exactly 0.5 represents unknown occupancy, and greater than 0.5 implies a probably of occupied space. They used Polaroid laboratory grade ultrasonic range transducers whose measuring range span distances from 0.9 to 35.0 ft. The main lobe of the sensitivity function is contained within a solid angle Ω of 30°, where it falls off to –38 dB. The beam width ω at –3 dB is approximately 15°. Range accuracy of the sensors is on the order of 1%. The associated control circuitry only reports the distance to the first strong reflector. The sonar sensor array consists of a ring of 24 transducers, spaced 15° apart. They are mounted in their Neptune mobile robot. In their experience, the robot surveyed a 30 by 15 feet indoor laboratory and built a 6 by 6 inches cell by combining the readings from successive vehicle stops made about one meter apart. The map update process extracts a reasonable world description from noisy data from different views and different sensors. They obtained successful, results whereby they treat different sensors uniformly, model uncertainty in the sensor data, and accommodate information over time. However, they use ad hoc statistical models and methods to construct a map under the assumption that sensor information is completely independent.

Cho[Cho90] improved the methodology. He relaxed the assumption and derived formulae from the Bayes's formula not based on the ad hoc approach. In order to

ascertain the validity of the preceding formulae, simulation has been performed and results were compared to the original map. He proved to be able to identify and modify the surroundings of robots quite accurately through simulation. Later, Lim and Cho[Lim96] modified probability density function by introducing orientation probability and applied this sensor model to the Bayes's updating formula. They equipped their mobile robot, GS-boy, with 9 ultrasonic sensors which have a detection range of 0.05 to 3m and IBM-AT compatible 80486 computer. In their experiment, the robot moves within a $3m \times 3m$ indoor room which consists of paper boxes, bookshelves, and walls. The dimension of the map is 80×76 cells with a cell size of $0.04 \times 0.04\ m^2$. The robot has a speed of 0.1 m/s at its steady state and 9 sets of range data are taken every 0.09m.

Borenstein and Koren[Bor89, Bor91a, Bor92b] changed the methodology to improve the robot's speed. The procedure using an uncertainty grid method with Bayes's formula is computationally intensive and imposes a heavy time penalty if a real-time execution on an on-board computer is attempted. They introduced the histogram instead of the probabilistic uncertainty to reduce the computational cost. This method, called Histogramic In-Motion Mapping, uses a two dimensional Cartesian histogram grid for obstacle representation. Like the certainty grid, each cell in the histogram grid holds an integer value that represents the confidence in the existence of an obstacle at that location. Only one cell which indicates the obstacle boundary is incremented and some cells which indicate free space are decreased for each range reading obtained by continuous and rapid sampling of the sensors while the vehicle is moving. For instance, with ultrasonic sensors, the cell indicating the obstacle boundary lies on the acoustic axis and corresponds to the measured distance and the cells indicating free space are located on the line connecting

the center cell and origin cell. Thus, the same cell and its neighboring cells are repeatedly incremented. The final map contains cell values. The greater the value in a cell, the greater the level of confidence that the cell is occupied by an obstacle. They equipped the CYBERMATION K2A mobile robot, CARMEL, with a ring of 24 Polaroid ultrasonic sensors and an additional computer (a PC-compatible single board computer, running at 7.16 MHz), to control the sensors. The sensor ring has a diameter of 0.8 m, and objects must be at least 0.27 m away from the sensors to be detected. Sensor information is evaluated on a 20 MHz IBM-AT compatible 80386 computer. In their experiment, the robot's work space area is 33×33 cells forming a window with a cell size of 10 cm $\times$ 10 cm, and the window is always centered about the vehicle's position. The vehicle moves within a 4 m $\times$ 4 m indoor room which consists of partitions, poles, and walls. The value of a cell ranges from 0 to 15. Free space and obstacles are separated by an arbitrary threshold. A two dimensional Cartesian histogram grid is continuously updated in real-time with range data sampled by the on-board range sensors. The local map is used for navigation to avoid obstacles by a virtual force field method or by a vector field histogram method. The average vehicle speed is 0.7 m/s without stop during sensing.

They also introduced an index of performance, designed to quantitatively express the match between a sensor-built map and a precisely measured reference map in order to compare the accuracy of different map building methods as well as the effect of different parameters with a certain method[Ras90].

Stuck and Manz[Stu94] also used the histogram grid map for path planning. However, a 3-D laser range finder is used instead of ultrasonic sensors. Although the laser range finder operates more slowly than the ultrasonic sensors, the data it provides

are more precise and offer a higher angular resolution at greater range. The 3-D laser range finder consists of two components: a sensor head, which holds a CCD camera with a modified lens incorporating a dual aperture iris and a laser projector that projects a vertical stripe of light, and a processing system. The head rotates as it acquires range data. The angular resolution is approximately 6.2° in the horizontal plane and the average range accuracy is about 0.7% at 2 m and 1.4% at 3 m. Since the vehicle moves as it acquires data, its position and orientation at each acquisition are different. To compensate for distortion, the vehicle's position is interpolated and data are corrected by using the interpolated positions. In their experiment, a cell size of 10 cm × 10 cm is used in the grid representation. The cell value ranges from 0 to 14 where a value of 7 indicates unknown. With path planning, the vehicle moves at 0.17 m/sec ~ 0.23 m/sec in a 6.0 m × 8.4 m indoor room consisting of desks, chairs, tables, boxes, and partitions.

There are two problems with the Bayes's approach. One is an assumption that cell values are independent; i.e., no relationship whatsoever exists between the states of two cells, even if they are adjacent. Second is the maximum entropy assumption that prior probabilities are typically 0.5.

Oriolo, Ulivi, and Vendittelli[Ori95, Pol95, Ori97, Ori98] applied fuzzy logic to a probabilistic uncertainty grid to solve the independence assumption. Sensors are modeled by using a membership function and the map is defined as fuzzy sets over the environment where a real value associated with each point quantifies its possibility of being occupied by an obstacle. To update the fuzzy map, a Dombi union operator, a bounded product, and a bounded sum are employed. 16 ultrasonic sensors which can detect distance from 11.5 to 650 cm with 1% accuracy and have 25° angular resolution

are equipped on a mobile robot, the Nomad 200.To increase measurement accuracy, at each position the ring is rotated twice by an angle of 7.5°. As a result, 48 range readings are obtained at each measurement location. In their experiment, a cell size of 10 cm × 10 cm is used in the grid representation. The cell values range from 0.0 to 1.0. A value of 0.5 indicates unknown. The vehicle surveyed in a 7.5 m × 10.0 m indoor room which consisted of walls and obstacles.

Zang and Webber[Zha92b, Zha96] offer a grid-based method for detecting moving objects. The occupancy grid method is extended to form the basis for a probabilistic estimation of the location and velocity of objects in the scene from the sensor data. The Hough transform is used to determine the velocities of the contents of the occupied cells. Under the assumption that objects in the environment are moving with constant velocity, they presented the simulation using a model of a ring of 24 ultrasonic sensors. However, they extract motion information from probabilistic sensor data ignoring the overlap of data which is necessary to re-enforce empty volumes.

Boundary Representation

In most applications of a grid model, navigation is performed in an indoor environment such as a room. However, navigation in an outdoor environment and global path planning require a large map area. As the area of space increases, the total cost using a grid model is proportional to $O(n^5)$ where n is the number of cells in a map. Thus, for path planning in an outdoor environment, a boundary representation is used for the description of the environment.

Rankin, Armstrong and Crane[Ran93, Ran94] used a polygon defined by the coordinates of each vertex in the world coordinate system and a circle defined by the coordinates of the center in the world coordinate system and the radius, which surround the forbidden regions. A global path from a stationary pose to a goal pose is generated from the map representation.

Rao[Rao95] used a generalized polygon which consists of a connected sequence of circular arcs and straight line segments to navigate a point robot in an unknown two dimensional terrain populated by disjoint generalized polygonal obstacles.

Liu and Arimoto[Liu92, Liu95] simulated path planning using a set of obstacles with arbitrary boundaries such as a polygon and a curve in a two dimensional environment. A map is given a priori and converted to a tangent graph to find an optimal path.

Simsarian, Olson and Nandhakumar[Sim96] assumed that the robot's environment is represented by a two dimensional map of polygonal objects. The map is decomposed into a view invariant region which is a visibility information that is implicit in the map for the robot's selflocalization.

Koch, Yeh, Hillel, Meystel and Isik[Koc85] used a two dimensional "bug world" with polygonal obstacles which are represented by a list of their vertices. In their simulation, the map is updated by obstacle addition, obstacle deletion, and obstacle modification under a strong assumption that the sensor subsystem has accurate ranging capabilities so that the information provided gives detailed obstacle locations and structure.

Ayache and Faugeras[Aya89] built and updated a three dimensional map of the indoor environment of a mobile robot that uses passive vision. Three dimensional lines are used as primitives which have a three dimensional uncertainty caused by a pixel uncertainty and calibration in the stereo vision. The direction of the line is a vector along the line with unit value of z axis, and the position of the line is the point of intersection of the line with the xy plane. Based on these primitives, geometric primitives such as a three dimensional surface are created with the uncertainty reduction considering the geometric relationship between them.

Zhang and Faugeras[Zha92a] improved the three dimensional line which is represented by two parameters for the orientation and three parameters for the position of a point on the segment. The proposed representation is simple and convenient to characterize the uncertainty of a segment. A Kalman filter is used to merge matched line segments.

Feature-based Model

A feature-based model represents objects explicitly as well as a boundary representation. Usually this model is used for localization of a vehicle using a landmark in the environment to correct the vehicle's position. Extracted features from sensor data are composed to given features in a map whose positions are known in advance.

Rencken[Ren93] used a map which consists of two types of features such as planes and corners for localization using ultrasonic sensors. A plane's state is represented by the hessian normal form of a finite line segment visible from one side. A corner's state is represented by the global Cartesian coordinates of a point. In the simulation, a robot's

task is to follow the wall of a $5 \times 5m^2$ indoor room. As the robot moves, features are built up and placed into the map.

Stein and Medioni[Ste95] used the panoramic horizon from a topographic map by computing a set of sample slices at equal angle around the location for localization. These horizon curves are approximated by polygons.

Betke and Gurvits[Bet97] used points belonging to doors, pictures and fire extinguishers as landmarks for a robot's localization in a two dimensional map of an indoor environment. The positions of points are represented by complex numbers and detected by a camera with a reflecting ball that provides "fish-eyed" circular images of the surroundings.

Talluri and Aggarwal[Tal96] used the polyhedral buildings' flat rooftops as the world model features in an outdoor urban, man-made environment. Building the edge visibility regions from the given world model description, the position and pose of the robot are estimated by establishing correspondence between the world model features, which are the buildings' rooftops, and the image features, which are lines extracted from the image.

Topological Graph

Topological graphs are expressed using higher level abstraction and can represent an environment with less information than other methods. Consequently, it simplifies the task of robot decision making. This representation is used for global path planning in large-scale spaces.

Deng and Mirzaian[Den96] used a graph map for the robot exploration problem. The environment consisted of nodes and edges. At each node, the robot can observe a consistent local relative orientation of its incident edges.

Multi-layered Representation

The concept of multi-layered representation has the benefit of being able to choose the most appropriate representation for the accomplishment of each task. However, because this implementation is computationally expensive and maintaining consistency between the representations is additionally required, in most of research, the vehicle which employs multi-layered representation remains stationary.

Elfes[Elf87a] described the multiple axes of the representation of a sonar map to use in different kinds of navigational tasks. The multiple axes are the abstraction axis, the geographical axis and the resolution axis. The abstraction axis has the sensor level using a probabilistic uncertainty grid, the geometric level using polygonal boundaries, and the symbolic level using a topological graph. Along this axis the quality of data changes from a sensor-based low-level data-intensive representation to increasingly higher levels of interpretation and abstraction. The geographical axis indicates the characteristics of the area such as views around the robot, local map, and global map. The resolution axis indicates the different values of grid resolution. Some computations can be performed satisfactorily at low level of details, while others have to be done at high degrees of resolution.

Brezetz, Chatila and Devy[Bre95] used two models which are a local model and a global model. A local model is computed from one perception, and a global model

corresponds to the environment perceived by the robot since the beginning of its movement. After each perception, the new local model is fused with the global model to update it. The local model includes the information on the objects and their relationships as perceived from one view, and its data structure consists of geometrical features such as center of mass, matrix of inertia, maximum of elevation and total area, topological relations, and a 3-D point list. The global model describes landmarks which have a salient maximum elevation. It is represented by a coarse description in terms of an ellipsoid and a more accurate description in terms of a superquadric with the topological relations between landmarks.

Horst[Hor96] offers a conversion method between two representations of a grid model and object boundary representation to maintain consistency between these representations. Especially, for conversion from a grid model to object boundary, image processing techniques, such as edge detection, thinning, curve tracking, and linear approximation are employed with various modifications. In this paper, he suggests that the certainty grid can be maintained as a local map and a set of obstacle boundary curves as a global map.

To summarize the literature review, the author has created the following tables to compare the current works. These tables will confirm the novelty and originality of this research which is discussed in the next chapter.

Table 2-1 Comparison of Previous Works

Title	High Resolution Maps from Wide Angle Sonar	Sensor Integration for Robot Navigation : Combining Sonar and Stereo Range Data in a Grid-Based Representation	Sensor Fusion in Certainty Grids for Mobile Robots	Certainty Grid Representation for Robot Navigation by a Bayesian Method
Author	Moravec, Elfes	Elfes, Matthies	Moravec	Cho
Topic	Map Building	Map Building	Map Building	Map Building
Environment	Indoor on a Flat Ground	Indoor on a Flat Ground	Indoor on a Flat Ground	Simulation
Object	Multiple, Stationary Unknown, Positive Geometric (Wall, Bookcase, Chair)	Multiple, Stationary Unknown, Positive Geometric	Multiple, Stationary Unknown, Positive Geometric	Multiple, Stationary Unknown, Positive Geometric
Sensor	A Ring of 24 Ultrasonic Sensors (0.9 - 35.0 ft)	A Ring of 24 Ultrasonic Sensors (0.9 - 35.0 ft) Stereo Vision (15° FOV)	A Ring of 24 Ultrasonic Sensors Stereo Vision	Simulated Range Measurement
Map Structure	Grid Model	Grid Model	Grid Model	Grid Model
Map Size	30 ft × 15 ft		25 m × 35 m	
Mapping Function	Obstacle Addition Free Space Addition	Obstacle Addition Free Space Addition	Obstacle Addition Free Space Addition	Obstacle Addition Free Space Addition
Method	Probabilistic Addition Formula	Bayesian Estimation	Bayesian Estimation	Bayesian Estimation
Robot Name	Neptune	Neptune	Neptune	
Velocity	Stop during Sensing		Stop during Sensing	

Table 2-2 Comparison of Previous Works

Title	Real-time Obstacle Avoidance for Fast Mobile Robots	A Comparison of Grid-type Map-building Techniques by Index of Performance	The Vector Field Histogram - Fast Obstacle Avoidance for Mobile Robots	Histogramic In-Motion Mapping for Mobile Robot Obstacle Avoidance
Author	Borenstein, Koren	Raschke, Borenstein	Borenstein, Koren	Borenstein, Koren
Topic	Navigation	Map Building	Navigation	Map Building
Environment	Indoor on a Flat Ground	Indoor on a Flat Ground	Indoor on a Flat Ground	Indoor on a Flat Ground
Object	Multiple, Stationary Unknown, Positive Geometric (Wall)	Multiple, Stationary Unknown, Positive Geometric (Pole,Box,Partition,Wall)	Multiple, Stationary Unknown, Positive Geometric (Pole, all)	Multiple, Stationary Unknown, Positive Geometric (Pole, Box, Partition, Wall)
Sensor	A Ring of 24 Ultrasonic Sensors (2 m max)	A Ring of 24 Ultrasonic Sensors	A Ring of 24 Ultrasonic Sensors (2 m max)	A Ring of 24 Ultrasonic Sensors (0.27 - 2 m range) (3 - 5 Hz Sampling)
Map Structure	Grid Model	Grid Model	Grid Model	Grid Model
Map Size	33×33 cells around Robot	5 m × 7 m	33×33 cells around Robot	4 m × 6 m
Mapping Function	Obstacle Addition	Obstacle Addition Free Space Addition	Obstacle Addition	Obstacle Addition Free Space Addition
Method	Histogram	Bayesian Estimation Histogram	Histogram	Histogram
Robot name	CARMEL		CARMEL	CARMEL
Velocity	0.6 - 0.8 m/s		0.6 - 0.8 m/s	0.6 - 0.8 m/s

Table 2-3 Comparison of Previous Works

Title	Map Updating and Path Planning for Real-time Mobile Robot Navigation	On-Line Map Building And Navigation for Autonomous Mobile Robots	Fuzzy Maps : A New Tool for Mobile Robot Perception and Planning	On Combining the Hough Transform and Occupancy Grid Methods for Detection of Moving Objects
Author	Stuck, Manz, Elgazzar	Oriolo, Vendittelli, Ulivi	Oriolo, Vendittelli, Ulivi	Zhang, Webber
Topic	Navigation	Navigation	Map Building	Map Building
Environment	Indoor on a Flat Ground	Indoor on a Flat Ground	Indoor on a Flat Ground	Indoor on a Flat Ground
Object	Multiple, Stationary Unknown, Positive Geometric (Pole,Box,Partition,Wall)	Multiple, Stationary Unkgown, Positive Geometric (Wall)	Multiple, Stationary Unknown, Positive Geometric (Wall,Cabinet)	Multiple Moving(const. Vel.) Unknown, Positive Geometric(rectangular)
Sensor	A Ring of 24 Ultrasonic Sensors (2 m max, 3 Hz sampling) 3-D Laser Range Finder (2 Cameras + Laser Projector)	A Ring of 16 Ulttasonic Sensors	A Ring of 16 Ultrasonic Sensors (48 Range Reading / Measure)	A Ring of 24 Ultrasonic Sensors Model (Simulation)
Map Structure	Grid Model	Grid Model	Grid Model	Grid Model
Map Size	6.0 m × 8.4 m	7.5 m × 10.0 m	18 m × 12 m	32 cell × 32 cell
Mapping Function	Obstacle Addition	Obstacle Addition	Obstacle Addition Free Space Addition	Obstacle Addition
Method	Histogram	Fuzzy Logic	Fuzzy Logic	Bayesian Estimation Hough Transform
Robot Name	eAVe	Nomad 200	Nomad 200	
Velocity	0.15 - 0.35 m/s	Stop during Sensing	13 sec for Map Building	

Table 2-4 Comparison of Previous Works

Title	Dynamic World Modeling for a Mobile Robot among Moving Objects	Navigation of an Autonomous Robot Vehicle	Path Planning and Path Execution Software for an Autonomous Nonholonomic Robot Vehicle	Robot Navigation in Unknown Generalized Polygonal Terrains Using Vision Sensors
Author	Zhang, Webber	Rankin, Armstrong, Crane	Rankin	Rao
Topic	Map Building	System	Path Planning	Path Planning
Environment	Indoor on a Flat Ground	Outdoor, unpaved ground	Outdoor, unpaved ground	Algorithm
Object	Multiple Moving(const. vel.) Unknown, Positive Geometric(rectangular)	Multiple, Stationary Unknown, Positive Natural shape	Multiple, Stationary Unknown, Pos/Neg Geometric (N-sided polygon)	Multiple, Stationary Unknown, Positive Geometric (Polygonal obstacle)
Sensor	A Ring of 24 Ultrasonic Sensor Model (Simulation)	A Ring of 16 Ultrasonic Sensors (7 m max) Map is given	Map is given	Vision Sensors
Map Structure	Grid Model	Boundary Representation	Boundary Representation	Boundary Representation
Map Size	32 cell × 32 cell			
Mapping Function	Obstacle Addition			Obstacle Addition Free Space Addition
Method	Bayesian Estimation Hough Transform		Modified A* Algorithm	Visibility graph Voronoi Diagram
Robot Name		NTV	NTV	
Velocity		1.0 - 7.0 mph	1.0 - 7.0 mph	

Table 2-5 Comparison of Previous Works

Title	Path Planning Using a Tangent Graph for Mobile Robots Among Polygonal and Curved Obstacles	Finding the Shortest Path of a Disc Among Polygonal obstacles Using a Radius-Independent Graph	View-Invariant Regions and Mobile Robot Self-Localization	Simulation of Path Planning for a System with Vision and Map Updating
Author	Liu, Arimoto	Liu, Arimoto	Simsarian, Olson	Koch,Isik,Yeh,Hittel
Topic	Path Planning	Path Planning	Localization	Navigation
Environment	Algorithm	Simulation	Simulation	Simulation
Object	Multiple, Stationary Unknown, Positive Geometric	Multiple, Stationary Unknown, Positive Geometric	Multiple, Stationary Unknown, Positive Geometric (Wall)	Multiple, Stationary Unknown, Positive Geometric
Sensor	Map is given	Map is given	Map is given	Simulated Range Sensor
Map Structure	Boundary Representation	Boundary Representation	Boundary Representation	Boundary Representation
Map Size				
Mapping Function				Obstacle Addition Obstacle Deletion Obstacle Modification
Method	Tangent graph	Extended Tangent graph	View-Invariant Region	
Robot Name				
Velocity				

Table 2-6 Comparison of Previous Works

Title	Maintaining Representations of the Environment of a Mobile Robot	A 3D World Model Builder with a Mobile Robot	Concurrent Localisation and Map Building for Mobile Robots Using Ultrasonic Sensors	Map-Based Localization Using the Panoramic Horizon
Author	Ayache, Faugeras	Zhang, Faugeras	Rencken	Stein, Medioni
Topic	Map Building	Map Building	Localization	Localization
Environment	Indoor on a Flat Ground	Indoor on a Flat Ground	Man made outdoor	Outdoor
Object	Multiple, Stationary Unknown, Positive Geometric (Table, Chair)	Multiple, Stationary Unknown, Positive Geometric (Table, Chair, Wall)	Multiple, Stationary Unknown, Positive Geometric (Polyhedral building)	Multiple, Stationary Unknown, Positive Geometric (Horizon)
Sensor	Stereo Vision	Three Cameraes for 3D World Model Ultrasonic Sensor for Obstacle Avoidance	One Camera 3D Map is given	Panoramic View
Map Structure	Boundary Representation	Boundary Representation	Feature-based Model	Feature-based Model
Map Size				21.17 km × 14.04 km
Mapping Function	Uncertainty Reduction	Uncertainty reduction		
Method	Extended Kalman Filter	Kalman filter	Edge Visibility Region	
Robot Name		INRIA		
Velocity		9 sec / process		

Table 2-7 Comparison of Previous Works

Title	Mobile Robot Localization Using Landmarks	Mobile Robot Self-Location Using Model-Image Feature Correspondence	Competitive Robot Mapping with Homogeneous Markers	Sonar-Based Real-World Mapping and Navigation
Author	Betke, Gurvits	Talluri, Aggarwal	Deng, Mirzaian	Elfes
Topic	Localization	Localization	Map Building	Navigation
Environment	Outdoor, unpaved ground	Indoor on a Flat Ground	Algorithm	Indoor on a Flat Ground
Object	Multiple, Stationary Unknown, Positive Natural shape (Rocks)	Multiple, Stationary Unknown, Positive Geometric (Door,Fire Extinguisher)	Markers	Multiple, Stationary Unknown, Positive Geometric
Sensor	3D Laser Range Finder	Camera+reflecting ball Global map is given		A Ring of 24 UltrasonicSensors (0.9 - 35.0 ft)
Map Structure	Feature-based Model	Feature-based Model	Topological Graph	Multilayered Representation
Map Size	30 m × 50 m	20 m × 20 m		20 ft × 30 ft
Mapping Function	Obstacle Addition	Landmark Detection	Node Addition	Obstacle Addition Free Space Addition
Method	Extended Kalman Filter			Probability Addition Formula
Robot Name	ADAM			Neptune
Velocity				

Table 2-8 Comparison of Previous Works

Title	Object-based Modelling and Localization in Natural Environments	Maintaining multi-level plannar maps in intelligent systems	Multipath Bayesian Map Construction Model from Sonar Data	Real-Time Map Building and Navigation for Autonomous Robots in Unknown Environments
Author	Brezetz,Chatila,Devy	Horst	Lim, Cho	Oriolo, Ulivi, Vendittelli
Topic	Localization	Map Management	Map Building	Map Building
Environment	Indoor on a Flat Ground	Indoor on a Flat Ground	Indoor on a Flat Ground	Indoor on a Flat Ground
Object	Multiple, Stationary Unknown, Positive Geometric	Multiple, Stationary Unknown, Positive Geometric	Multiple, Stationary Unknown, Positive Geometric (Wall, Box, Shelf)	Multiple, Stationary Unknown, Positive Geometric (Wall, Desk, Shelf)
Sensor	A Ring of 24 Ultrasonic Sensors Model (Simulation)	Simulation Map is given	9 Ultrasonic Sensors	A Ring of 16 Ultrasonic Sensors
Map Structure	Multilayered Representation	Multilayered Representation	Grid Model	Grid Model
Map Size	5 m × 5 m	256 pixel × 256 pixel	3m × 3m	7.6m × 6.3m
Mapping Function	Obstacle Addition	Representation Conversion	Obstacle Addition Free Space Addition	Obstacle Addition Free Space Addition
Method		Modified Image Processing	Bayesian Estimation	Fuzzy Logic
Robot Name			GS-boy	Nomad 200
Velocity			0.1 m/s	0.25 sec stop / sensing

CHAPTER 3
MAP MANAGEMENT SYSTEM

Statement of Problem

The following overall problem statement is presented here.

Given: (1) Accurate three dimensional position and orientation of a mobile vehicle.
(2) Range data from ultrasonic sensors and/or a laser range scanner.
(3) A car-like vehicle as a platform that is controlled with velocity and steering angle commands.
(4) Three dimensional objects and terrain.

Develop: A multi-layered map management system which can detect obstacles around a vehicle and build a map for a large-scale outdoor environment while a vehicle is moving.

The system consists of local grid map management and global contour map management. The local grid map management will be able to fuse data from different sensors and update the local grid map over time with uncertainty reduction to detect obstacles around the vehicle. The global contour map management will be able to produce a polygon approximation of probability contour by using data that come from the local grid map to reduce the volume of global map data. The global contour map will also initialize the local grid map by using previous contour data when the vehicle returns to previously visited locations.

In this research, a multi-layered map management system will be evaluated in simulation comparing the results with several other sensor modeling and update formulae for the local grid map. A program will be written to create a simulated three dimensional environment, a vehicle, and range sensors.

The remainder of this dissertation will describe the author's work in accomplishing these tasks.

Assumptions

The environment and characteristics of information used in this research are specified by the performance of the sensors used. The following assumptions are made:

1. Accurate position and orientation data can be obtained for the vehicle. To obtain accurate position and orientation, many researchers who study navigation utilize a variety of sensors and methods. For an outdoor vehicle, it is common to use a Differential Global Positioning System. The sensor-related positioning errors are not considered here.
2. Obstacles are unknown, multiple, positive, and natural shaped objects in an outdoor environment. They are also stationary. Unknown objects are objects which are not described previously. Multiple objects means that several objects are in one field of view of a sensor. Positive objects are convex objects such as trees and rocks. Negative objects like ditches are not considered.
3. A limited sensing field of view, different sampling times, and resolutions are considered as performance parameters of ultrasonic and laser range sensors.
4. The vehicle is operated in a simulated environment which consists of three dimensional terrain and positive objects. It is controlled by speed and steering angle commands.

Research Requirements

The goal of this research was to develop a multi-layered map management system. To meet this goal, the author developed the system architecture shown in Figure 3-1.

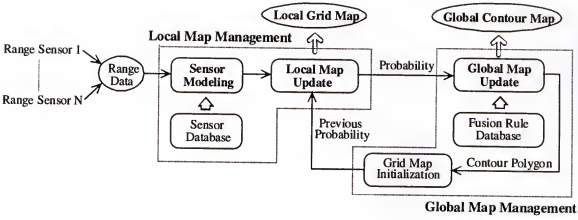

Figure 3-1 Multi-layered Map Management System

The developed system consists of three main components: sensor modeling, local map management, and global map management. The system obtains range data from ultrasonic sensors and a laser range scanner. These sensors have a variety of performances and characteristics as described in chapter 1. Range data from these sensors are the distances between the sensor and the closest point of obstacles in the field of view. Hence, it is possible that range data from the different sensors can be expressed uniformly. Sensor modeling is required to model range data into uniform data and this modeling includes uncertainty caused by noise poor sensor performance. Therefore, uncertainty needs to be described in the uniform data structure.

Using a sequence of uniform data, local map management must reduce uncertainty by updating a value in grid cell and produce a local grid map around the vehicle. The origin of the local grid map is the vehicle's position and the coordinate axes associated with the grid are north and east instead of being parallel to the vehicle's coordinate system. Updating the map is complex and difficult due to limited sensing space and time

while a vehicle is moving. The development of a map update formula is most crucial element of local map management.

The local grid map moves with the vehicle and values will "fall out of" the grid as the vehicle moves. The global map management system collects those data, generates polygons, and produces a global contour map relative to a coordinate system whose origin is the starting point of the vehicle and whose axes are north and east. Global map management is required to reduce the volume of data by converting from grid data to polygon data and to update polygonal contours. Also, conversion from polygon data to grid data is done to initialize the grid map during the grid map initialization process.

Contributions

The main contribution of this research is the development of a two dimensional map for a large-scale outdoor environment, which technically includes

1. developing sensor modeling using fuzzy concept to describe the uncertainty in sensor data and to deal with different range sensors uniformly that have different performance characteristics,
2. developing new formula of sensor fusion and map update for local grid map to reduce the uncertainty,
3. updating the contour map while a vehicle is moving,
4. initializing the local grid map by using previous contour data when the vehicle returns to a previously visited location.

Moreover, this research would be of benefit to an autonomous vehicle. For an autonomous vehicle, the map and positions of the vehicle can be used for navigation, path

planning, and world modeling. During navigation, the local grid map will be used for collision avoidance. Path planning will use it for path generation. World modeling will use the map for obstacle identification.

A map is the fundamental information of an environment. Therefore, potential application areas for an autonomous vehicle equipped with this map management system are surveillance of a hazardous area, and exploration of other planets where a communication signal delay makes direct human contact difficult. On the other hand, in a commercial area, car navigation systems and intelligent vehicle highway systems are developing. To summarize the applications, the author has created the figure shown in Figure 3-2.

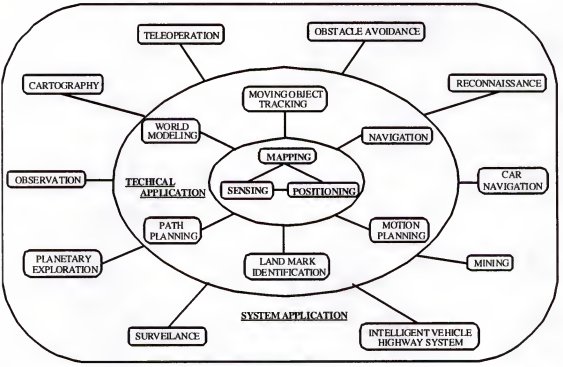

Figure 3-2 Applications for Multi-layered Map Management System

CHAPTER 4
DISCUSSION OF LOCAL GRID MAP UPDATE METHODS

In chapter 2, a variety of sensor models and update methods for a grid model are reviewed as previous works. In the literature, the word uncertainty appears many times. However, there is no discussion about the concept of uncertainty. In this chapter, the concept of uncertainty is investigated and previous works are discussed from the viewpoint of uncertainty as a bridge to chapter 5.

Concept of Uncertainty

In a daily life, many events are observed everywhere. In science, scientists have been striving to represent prime elements by observing data qualitatively and quantitatively, and to discover principles by finding the relationship between them. Until the late 19^{th} century, many scientists believed that every phenomenon could be expressed and predicted with certainty and that uncertainty is undesirable in science and should be avoided by all possible means. With the process of atomic physics, however, they realized that uncertainty is essential to science involving the development of quantum mechanics.

Websters' II New College Dictionary defines uncertain as "Not known or established," "Not determined" and "Not having sure knowledge." From the viewpoint of information science, uncertainty is characterized by three types; randomness, fuzziness and indeterminacy [Leh96, Nea96].

Random is defined in Websters' II New College Dictionary as "Of designating an event having a relative frequency of occurrence that approaches a stable limit as the number of observations of event increases to infinity." For example, it is impossible to predict with certainty the occurrence of heads for the single toss of a balanced coin. Such random events cannot be predicted with certainty, but the relative frequency with which they occur in a long series of trials is often remarkably stable. Events possessing this property are called random or stochastic events. This stable, long-term relative frequency provides an intuitively meaningful measure of one's belief in the occurrence of a random event for a future observation. To deal with randomness in uncertainty, there is a probability theory that is a branch of mathematics that studies the likelihood of occurrence of random events for the purpose of predicting the behavior of defined systems. The fundamental axiom is that of additivity of the probabilities of disjoint events [Wac95, Kyb96].

Fuzziness is not a priori an obvious concept and demands some explanation. "Fuzziness" is what Max Black in 1937, who is the American philosopher, calls "vagueness" when he distinguishes it from "generality" and from "ambiguity." Generalizing refers to the process of abstraction to a multiplicity of objects in the field of reference, ambiguity to the association of a finite number of alternative meanings of words having the same phonetic form. But the fuzziness of a symbol lies in the absence of well-defined boundaries of the set of objects to which this symbol applies. Lofti A. Zadeh introduced a fuzzy logic theory whose objects -fuzzy sets- are sets with boundaries that are not precise. The membership in a fuzzy set is not a matter of affirmation or denial, but

rather a matter of a degree. Fuzzy control is one of the most successful applications of the fuzzy logic theory [Dub80, Dri93, Kli95, Lew97, Ngu95].

Indeterminacy is defined in Websters' II New College Dictionary as "Not precisely determined" and "Not known in advance." For example, assume you are a student who is uncertain about the true or false answer of a question. Because the question itself has very distinct boundaries, that is an answer, this uncertainty is not fuzziness. If you do not have knowledge about the question, you would say the true and false are fifty-fifty percent and choose either true or false as your answer at random. It sounds like randomness in uncertainty. But if you have some imperfect knowledge and you think the answer could be true, you will have higher belief of true than of false and you choose true as your answer. This type of uncertainty representing degree of belief is called indeterminacy. That is, though things have crisp results, you cannot determine which one is in advanced because of imperfect knowledge or less evidence. Instead you will assign a value to each thing signifying the degree of evidence or belief. Hence, the numerical value of the probability is interpreted as a measure of the feeling of uncertainty. Obviously, different from randomness, a belief is a property of a single trial and a subjective judgment. To deal with indeterminacy, there are evidence theory, possibility theory, and fuzzy measure that are offspring of classical measure theory developed by Émile Borel, a French mathematician.

In the context of probability theory, a generalized theory based on two types of nonadditive measures was originated by Dempster and, later, fully developed by Shafer. With the development of classical measure theory, additivity that the value for a bounded union of a sequence of pairwise disjoints sets is equal to the sum of the values associated

with the individual sets becomes too restrictive to capture adequately the full scope of measurement. Instead non-additive measures are introduced by replacing the additivity requirement of probability measures with either a superadditivity requirement or a subadditivity requirement. The super-additive measures, which are also upper semicontinuous, are usually called belief measures. The subadditive measures, which are also lower semicontinuous, are usually referred to as plausibility measures. Given a measure of either of the two types, it induces a unique measure of the other type. Taken together, belief and plausibility measures form a theory that is usually called evidence theory or Dempster-Shafer theory. In the theory, the belief measures are used for a degree of a belief among the subsets of a frame of discernment. Two belief measures obtained in the same context from two independent sources are combined by Dempster's rule of combination to obtain a joint basic assignment [Mur98, Pag98, Zad86].

Possibility theory [Dub88, Del98] based on nonadditive measures emerged from the concept of a fuzzy set, which was proposed by Zadeh. In possibility theory, the uncertainty of an event is described both by the degree of possibility of the event itself and by the degree of possibility of the contrary event, these two measures being but weakly related. The complement with respect to 1 of the possibility of the contrary event can be interpreted as the degree of necessity of the event itself. Necessity measures and possibility measures whose focal elements are required to be nested in the possibility theory are special counterparts of belief measures and plausibility measures in evidence theory, respectively. The truth value of a proposition can be regarded as a measure and fuzzy logic operators or Dempster's rule of combination are used to combine degrees of uncertainty.

Fuzzy measures [Ral96, Wan92, Sme81, Gra95], according to Sugeno, are obtained by replacing the additivity requirement of classical measures with weaker requirements of monotonicity with respect to set inclusion and continuity. The requirement of continuity was later found to be still too restrictive and was replaced with a weaker requirement of semicontinuity. In fact, belief and plausibility measures, as well as necessity and possibility measures, are only semicontinuous. Fuzzy integral is used as an aggregation tool.

The following section, current map update formulas with sensor modeling are discussed from the viewpoint of uncertainty and the theory.

Probability Theory Approach

The poor performance of a sensor is regarded as randomness in certainty. Moravec and Elfes[Mor85, Mor88] at Carnegie Mellon University modeled a sonar beam by probability density function that satisfies the following definition 4-1.

Definition 4-1

Suppose that an experiment is associated with a sample space S. To every event A in S (A is subset of S) we assign a number, $P(A)$, called the probability of A, so that the following axioms hold:

Axiom 1: $P(A) \geq 0.0$

Axiom 2: $P(S) = 1.0$

Axiom 3: If $A_1, A_2, A_3 \ldots$ form a sequence of pairwise mutually exclusive events in S, then $P(A_1 \cup A_2 \cup A_3 \cup \ldots) = \sum_{i=1}^{\infty} P(A_i)$.

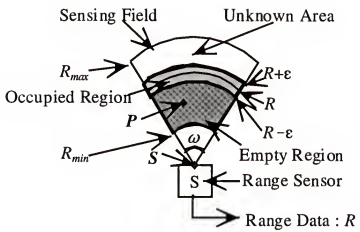

Figure 4-1 Range Sensor Performance

A range reading is interpreted as providing information about space volumes that are either empty or occupied. For generalization, performance parameters of the range sensor are modeled as shown in Figure 4-1. The following notations are used as the character of range sensors in the later discussion.

Let

R be the range measurement returned by the range sensor

R_{min} be the minimum measurement

R_{max} be the maximum measurement

ε be the mean deviation error of the range value

ω be the beam aperture

$\boldsymbol{S}$ be the position of the range sensor

$\boldsymbol{P}$ be a position within sensing field of the range sensor

δ be the distance from $\boldsymbol{P}$ to $\boldsymbol{S}$

θ be the angle between the main axis of the range sensor and $\boldsymbol{SP}$

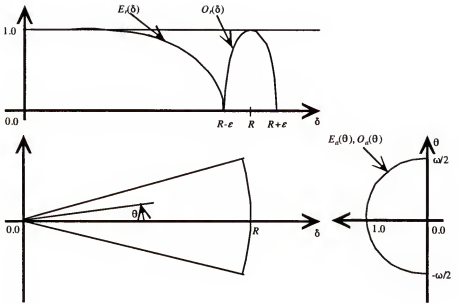

Figure 4-2 Probability Density Function

Two regions in the sensor beam are defined in a sensor coordinate system based on geometry of the beam and the spatial sensitivity pattern. The empty region is the region whose points are inside the sensor beam, that have a probability $P_E = f_E(\delta,\theta)$ of being empty. The empty probability density function for a point P inside the sensor beam is given by

$$P_E = f_E(\delta,\theta) = E_r(\delta) \cdot E_a(\theta) \tag{4.1}$$

where

$E_r(\delta) = 1 - ((\delta - R_{min}) / (R - \varepsilon - R_{min}))^2$ for $\delta \in [\, R_{min}, R-\varepsilon \,]$

$E_r(\delta) = 0$ otherwise

$E_a(\theta) = 1 - (2\theta/\omega)^2$ for $\theta \in [\, -\omega/2, \omega/2 \,]$

A single measure provides the information of obstacle distance with $\pm\varepsilon$ accuracy over the entire range. E_r indicates that probability of emptiness becomes lower as it is

close to occupied region and become zero at the border of empty region. Wave intensity decrease far from the beam axis and reaches zero at the border of lobe. The weight due to the angle from the beam axis is distributed by E_a, according to the semicircular shape.

The occupied region is the region whose points have a probability $P_O = f_O(\delta,\theta)$ of being occupied. The occupied probability density function for a point $\boldsymbol{P}$ on the beam front is given by

$$P_O = f_O(\delta,\theta) = O_r(\delta) \cdot O_a(\theta) \tag{4.2}$$

where

$O_r(\delta) = 1 - ((\delta - R) / \varepsilon)^2$ for $\delta \in [R - \varepsilon, R + \varepsilon]$

$O_r(\delta) = 0$ otherwise

$O_a(\theta) = 1 - (2\theta/\omega)^2$ for $\theta \in [-\omega/2, \omega/2]$

O_r indicates that the weight due to the distance is distributed according to the parabolic shape and reaches zero at the border of the region. O_a is the same role as E_a. The probability density functions are shown in Figure 4-2.

After producing the probability density functions for every sensor, they are projected onto the cell of a grid map defined in a global coordinate system. To distinguish from a sensor coordinate system, the notations for probabilities after transformation to a global coordinate system are written as $P_E(X,Y)$ for emptiness and $P_O(X,Y)$ for occupancy, respectively.

For a map update, probability theory was used regarding uncertainty of a sonar sensor as randomness. Each cell has two random variables such as a probability of free space, $P_{Emp}(X,Y)$, and a probability of obstacles, $P_{Occ}(X,Y)$, where X,Y are the position in

a global coordinate system. $P_{Emp}(X,Y)$ and $P_{Occ}(X,Y)$ are updated by an additive law of probability using both $P_E(X,Y)$ and $P_O(X,Y)$ from all range sensors.

Theorem 4-1 The Additive Law of Probability

The probability of the union of two events A and B is

$$P(A \cup B) = P(A) + P(B) - P(A \cap B). \tag{4.3}$$

If A and B are independent events, $P(A \cap B) = P(A) \cdot P(B)$ and

$$P(A \cup B) = P(A) + P(B) - P(A) \cdot P(B). \tag{4.4}$$

If A and B are mutually exclusive events, $P(A \cap B) = 0$ and

$$P(A \cup B) = P(A) + P(B). \tag{4.5}$$

Utilizing the additive law, it was assumed that probabilities in previous map and probabilities from sensors are independent from each other, $P(A|B) = P(A)$, and there is no modification of probabilities from sensors by using previous map information. The evidence combination proceeds along the following steps:

1. Reset: The whole map is set to unknown by making $P_{Emp}(X,Y) := 0$ and $P_{Occ}(X,Y) := 0$.
2. Superposition of empty areas: For every sonar reading, modify the emptiness information over its projection by

$$P_{Emp}(X,Y) := P_{Emp}(X,Y) + P_E(X,Y) - P_{Emp}(X,Y) \cdot P_E(X,Y). \tag{4.6}$$

3. Superposition of occupied area: For each reading, shift the occupied probabilities around in response to the combined emptiness map using:

$$P_O(X,Y) := P_O(X,Y) \cdot (1 - P_{Emp}(X,Y)) \tag{4.7}$$

$$P_O(X,Y) := P_O(X,Y) / \Sigma P_O(X,Y) \tag{4.8}$$

$$P_{Occ}(X,Y) := P_{Occ}(X,Y) + P_O(X,Y) - P_{Occ}(X,Y) \cdot P_O(X,Y). \quad (4.9)$$

4. Thresholding: The final occupation value attributed to a cell is given by a thresholding:

$$\begin{cases} P_{Occ}(X,Y) & \text{if } P_{Occ}(X,Y) \geq P_{Emp}(X,Y) \\ -P_{Emp}(X,Y) & \text{if } P_{Occ}(X,Y) < P_{Emp}(X,Y) \end{cases} \quad (4.10)$$

Bayes's Theorem Approach

Instead of using two random variables to update a map, one random variable was used to express the probability of occupancy for each cell by Elfes and Matthies[Elf87b], Cho[Cho90], and Lim and Cho[Lim96]. The value close to 0 indicates low probability of occupancy, which is high probability of emptiness. The value 0.5 is used as unknown and the value close to 1.0 indicates high probability of occupancy. Therefore, the same probabilistic sensor model described in probability theory approach is used with the following transformation.

$$P = f(\delta,\theta) = \begin{cases} 0.5 - f_E(\delta,\theta)/2 & \text{for } \delta \in [R_{\min}, R-\varepsilon] \text{ and } \theta \in [-\omega/2, \omega/2] \\ 0.5 + f_O(\delta,\theta)/2 & \text{for } \delta \in [R-\varepsilon, R+\varepsilon] \text{ and } \theta \in [-\omega/2, \omega/2] \end{cases} \quad (4.11)$$

Theorem 4-2 Bayes's Theorem

Assume that $S = B_1 \cup B_2 \cup \ldots \cup B_k$ where $P(B_i) > 0$, for $i = 1, 2, \ldots, k$ and $B_i \cap B_j = \phi$ for $i \neq j$, then $P(B_j \mid A) = \dfrac{P(B_j) \cdot P(A \mid B_j)}{\sum_{i=1}^{k} P(B_i) \cdot P(A \mid B_i)}$.

To utilize Bayes's theorem for a map update, it was assumed there are two states in an environment; obstacle, $\{A_O\}$, and free space, $\{A_F\}$. A probabilistic sensor model was regarded as a conditional probability density function P(sensor reading R | state of

environment, $\{A_O\}$ or $\{A_F\}$). For additional simplification, it was assumed that $P(R \mid \{A_F\}) = 1.0 - P(R \mid \{A_O\})$.

Let S be $S = \{A_F\} \cup \{A_O\}$ and $\{A_F\} \cap \{A_O\} = \phi$, from Bayes's theorem

$$P(\{A_O\} \mid R) = \frac{P(\{A_O\}) \cdot P(R \mid \{A_O\})}{P(\{A_O\}) \cdot P(R \mid \{A_O\}) + P(\{A_F\}) \cdot P(R \mid \{A_F\})} \tag{4.12}$$

Using complement, that is $P(\{A_F\}) = 1.0 - P(\{A_O\})$, and the additional simplifying assumption,

$$P(\{A_O\} \mid R) = \frac{P(\{A_O\}) \cdot P(R \mid \{A_O\})}{P(\{A_O\}) \cdot P(R \mid \{A_O\}) + (1 - P(\{A_O\})) \cdot (1 - P(R \mid \{A_O\}))} \tag{4.13}$$

$P(\{A_O\})$ is assigned to the previous value of $P(\{A_O\} \mid R)$ and initial value of $P(\{A_O\})$ is 0.5 as unknown. $P(R \mid \{A_O\})$ is given by the probabilistic sensor model. The desired probability is $P(\{A_O\} \mid R)$ as a updated value. Therefore the equation is rewritten as

$$P_{Occ}(X,Y) = \frac{P_{Occ}(X,Y) \cdot P(X,Y)}{P_{Occ}(X,Y) \cdot P(X,Y) + (1 - P_{Occ}(X,Y)) \cdot (1 - P(X,Y))} \tag{4.14}$$

Histogram Method Approach

To avoid real number calculation for real-time execution by an on-board computer, Borenstein and Koren [Bor89, Bor91a, Bor91b] at the University of Michigan separated the denominator part from the probability density function by regarding it as a maximum certainty value. Changing the value, the probability density function also changes. Therefore, it is possible to tune the sensor model according to the performance of range sensors and the condition of environment. Moreover, the probability density function itself was simplified as shown in Figure 4-3. It seems to be

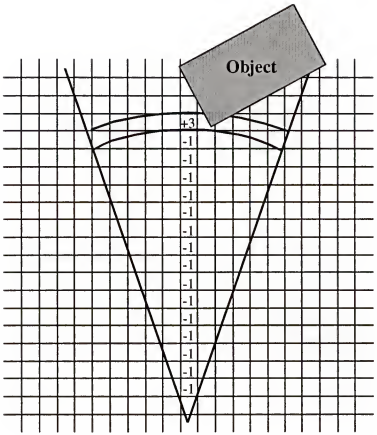

Figure 4-3 Histogramic Probability Distribution

different from probability theory, but from the viewpoint of the uncertainty concept, the histogram method is a kind of probability theory by devising the computational clue. The relationship between the probability density function and the histogramic probability distribution is as follows.

$$\begin{cases} P_O'(X,Y) := (\text{Increment step value}) / (\text{Maximum certainty value}) \\ P_E'(X,Y) := |\,\text{Decrement step value}\,| / (\text{Maximum certainty value}) \end{cases} \tag{4.15}$$

An ultrasonic sensor is modeled by a histogramic probability distribution. Information on the empty sector between R_{min} and $R - \varepsilon$ has the value for decrement all

cells along the main axis of the beam. Only one cell has the value for increment. The step value of increment and decrement were determined experimentally.

For map update procedure, two random variables such as $P_{Occ}'(X,Y)$ for occupancy and $P_{Emp}'(X,Y)$ for emptiness are used like in the probability theory approach. $P_O'(X,Y)$ for the occupied region and $P_E'(X,Y)$ for the empty region are produced every sensor reading using the histogramic probability distribution. It was assumed that two previous cell values, $P_{Occ}'(X,Y)$ and $P_{Emp}'(X,Y)$, and two step values from sensor, $P_O'(X,Y)$ and $P_E'(X,Y)$, are not only independent but also mutually exclusive, that is $P(A|B) = P(B|A) = 0$. Therefore, utilizing the additive law of probability the update formula is

$$\begin{cases} P_{Occ}'(X,Y) := P_{Occ}'(X,Y) + P_O'(X,Y) \\ P_{Emp}'(X,Y) := P_{Emp}'(X,Y) + P_E'(X,Y) \end{cases} \tag{4.16}$$

The final occupation value attributed to a cell is given by $P_{Occ}'(X,Y) - P_{Emp}'(X,Y)$.

In their experiment using CAMEL, whenever a cell is incremented, the increment is actually 3 and the maximum certainty value of a cell is limited to 15. Decrement, however, take place is steps of –1 and the minimum value is 0. The maximum and the minimum certainty value have been chosen arbitrarily. A threshold value of 12 was used to make a decision of the existence of obstacles from their experiment.

Fuzzy Logic Approach

In discussions above, it was assumed that uncertainty of range data is randomness and sensor modeling and map update procedures are based on probability theory. Oriolo, Vendittelli and Ulivi [Ori95, Ori97, Ori98], however, assumed that uncertainty of range

data attributed to vagueness of the boundary of the sensing field and utilized fuzzy logic. In sensor modeling, a membership function is used instead of a probability density distribution.

The influence of reflection is considered explicitly because reflections reduce certainty about the status of the explored cells. As reflected beams take a longer path than direct ones, the simplest way to deal with this phenomenon is to gradually reduce certainty from a maximum to a minimum according to the distance δ.

$$E_f(\delta) = \min(\, 1, h_1 \cdot \exp(-h_2 \cdot \delta) + h_3 \,) \quad \text{for } \delta \in [\, R_{min}, R-\varepsilon \,] \tag{4.17}$$

$$O_f(\delta) = \min(\, 1, h_1 \cdot \exp(-h_2 \cdot \delta) + h_3 \,) \quad \text{for } \delta \in [\, R-\varepsilon, R+\varepsilon \,] \tag{4.18}$$

Parameter h_3 represents the minimum degree of certainty, h_1 and h_2 are used to interpolate between the two values and take into account average distances in the environment.

Two coefficients, k_e and k_o, are added as the weight of the elementary acquisition for emptiness and occupancy. As a consequence, membership functions are defined as follows.

$$\mu_E = g(\delta,\theta) = k_e \cdot E_f(\delta) \cdot E_r(\delta) \cdot E_a(\theta) \tag{4.19}$$

$$\mu_O = g(\delta,\theta) = k_o \cdot O_f(\delta) \cdot O_r(\delta) \cdot O_a(\theta) \tag{4.20}$$

Membership functions are projected to the grid map using the position and yaw angle of the vehicle and the direction of main axis of the sensors. To distinguish from the sensor coordinate system, $\mu_E(X,Y)$ and $\mu_O(X,Y)$ are used for the grid map coordinate system.

For a map update, a degree of certainty is increased non-linearly using a fuzzy union operation like the increment in the histogram method.

Definition 4-2: Fuzzy Union Axiom u: $[0,1] \times [0,1] \rightarrow [0,1]$

1) Boundary condition $u(a,0) = a$
2) Monotonicity $b \leq d$ implies $u(a,b) \leq u(a,d)$
3) Commutativity $u(a,b) = u(b,a)$
4) Associativity $u(a, u(b,d)) = u(u(a,b), d)$

The pieces of information concerning the empty and the occupied cells are separately collected during the measuring process. The associative property of fuzzy union allows using two fuzzy sets $\mu_{Emp}(X,Y)$ and $\mu_{Occ}(X,Y)$ as accumulators. For the membership function for emptiness, $\mu_{Emp}(X,Y) = \bigcup \mu_E(X,Y)$ and for the membership function for occupancy, $\mu_{Occ}(X,Y) = \bigcup \mu_O(X,Y)$. For the accumulation of the degree of certainty, Dombi's union operation, whose strength can be varied by tuning a parameter λ, was used.

$$u_\lambda(\mu_A(x), \mu_B(x)) = \frac{1}{1+\left[\left(\frac{1}{\mu_A(x)}-1\right)^{-\lambda} + \left(\frac{1}{\mu_B(x)}-1\right)^{-\lambda}\right]^{-\frac{1}{\lambda}}} \qquad (4.21)$$

The chosen union family reaches certainty asymptotically and the operator produces larger union sets as λ is decreased; that is, weaker unions are obtained for small values of λ.

To decide free space from $\mu_{Emp}(X,Y)$ and $\mu_{Occ}(X,Y)$, a fuzzy intersection operator and a fuzzy complement operator are used.

Definition 4-3: Fuzzy intersection axiom i: $[0,1] \times [0,1] \rightarrow [0,1]$

1) Boundary condition $i(a,1) = a$
2) Monotonicity $b \leq d$ implies $i(a,b) \leq i(a,d)$
3) Commutativity $i(a,b) = i(b,a)$
4) Associativity $i(a, i(b,d)) = i(i(a,b), d)$

Definition 4-4: Fuzzy complement axiom c: $[0,1] \rightarrow [0,1]$

1) Boundary conditions $c(0) = 1$ and $c(1) = 0$
2) Monotonicity for all $a,b \in [0,1]$ if $a \leq b$ then $c(a) \geq c(b)$

Formula of free space decision is

$$\mu_{Emp}(X,Y) \cap \overline{\mu_{Occ}}(X,Y) \cap \overline{\mu_{Emp}(X,Y) \cap \mu_{Occ}(X,Y)}.$$

$\mu_{Emp}(X,Y) \cap \mu_{Occ}(X,Y)$ represents the set of cells for which the measures are ambiguous, with the membership values giving a degree of contradiction. For the fuzzy complement, the standard complement described in Definition 4-4, $c(A(x)) = 1 - A(x)$, was selected. For fuzzy intersection described in Definition 4-3, the standard intersection, $i(A(x) \cap B(x)) = \min(A(x), B(x))$ was used.

CHAPTER 5
MAP UPDATE UTILIZING THE MARKOV CHAIN APPROACH

The construction of a suitable sensor model is one of the most crucial issues for overall performance to reduce uncertainty. As discussed in chapter 4, sensor models in previous works are defined by the geometry of the beam and the spatial sensitivity pattern of the sensor. A typical sensor model has a distribution of higher probabilities near the center line axis of the sensor and relatively low probabilities on either side. It describes the uncertainty caused by the poor performance of sensors, but range data are also influenced by noise and sensor-environment interaction. Some models are modified by adding adjustable parameters like a maximum certainty value in the histogram method approach and weights in the fuzzy logic approach to produce a suitable model. However, it is very difficult to justify a particular probability profile considering the sensor has to work in varied, unknown environments.

The author has developed a new sensor model by using a fuzzy approach to describe uncertainty in range sensors. In this chapter, fuzzy modeling is introduced to describe uncertainty and a new map update formula utilizing a nonhomogeneous Markov Chain are developed using a fuzzy model to reduce uncertainty.

Fuzzy Modeling

A map is required to have information of obstacles and free space. Hence, the environment around a vehicle is characterized by two states that are obstacle and free space.

Ultrasonic sensors and laser range scanners are generalized as range sensors. Range sensors are characterized by the performance shown in Figure 5-1. Sensor signals are no data or range data that indicates the closest distance between a vehicle and obstacles within the sensing field. The value of range data, R, exists between minimum range, R_{min}, and maximum range, R_{max}. Information of free space in range data is either the entire sensing field when there are no data or the area between the obstacle and the sensor when there is a range value. It is assumed that the area behind obstacles is unknown. Sensor signals have uncertainty such as randomness caused by noise and fuzziness caused by poor resolution.

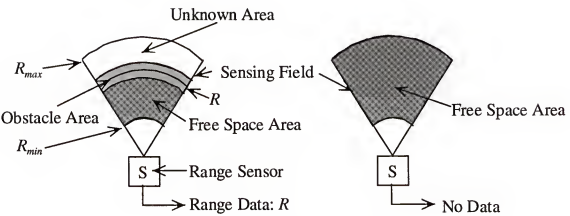

Figure 5-1 Range Sensor

To describe uncertainty in range data, three prime elements are defined as a frame of discernment Θ.

$$\Theta = \{A_O, A_F, A_N\}$$

where A_O: Obstacle in an environment

A_F: Free Space in an environment

A_N: Noise in a sensor

Taking the power set of Θ, the following set of all subsets of Θ is obtained.

$X = 2^{\Theta} = \{\{\phi\}, \{A_O\}, \{A_F\}, \{A_N\}, \{A_O, A_F\}, \{A_O, A_N\}, \{A_F, A_N\}, \{A_O, A_F, A_N\}\}$

Each element represents a component in the world as follows.

$\{\phi\}$: No environment and no noise in a sensor

$\{A_O\}$: Obstacle and no noise in a sensor

$\{A_F\}$: Free space and no noise in a sensor

$\{A_N\}$: No environment and noise in a sensor

$\{A_O, A_F\}$: Obstacle and free space and no noise in a sensor

$\{A_O, A_N\}$: Obstacle and noise in a sensor

$\{A_F, A_N\}$: Free space and noise in a sensor

$\{A_O, A_F, A_N\}$: Obstacle, free space and noise in a sensor

$\{\phi\}$, $\{A_N\}$, $\{A_O, A_F\}$ and $\{A_O, A_F, A_N\}$ are excluded because of the contradiction of existence in a real world. Therefore, $X = \{\{A_O\}, \{A_F\}, \{A_O, A_N\}, \{A_F, A_N\}\}$ is used as the universe of discourse.

Definition 5-1

Let X be a nonempty set considered as the universe of discourse, whose generic elements are denoted x. A fuzzy set A in X, that is a subset of X that has no sharp

boundary, is characterized by a membership function $\mu_A: X \rightarrow [0,1]$. The closer the value of $\mu_A(x)$ is to 1, the more x belongs to A. A is completely characterized by the set of pairs.

$$A = \{(x, \mu_A(x)), x \in X\}.$$

When X is a finite set $\{x_1, \ldots, x_n\}$, a fuzzy set on X is expressed as

$$A = \mu_A(x_1)/x_1 + \ldots + \mu_A(x_n)/(x_n) = \sum_{i=1}^{n} \mu_A(x_i)/x_i \tag{5.1}$$

As described in probability density function in probability theory approach, sensor data have information of empty area and occupied area. Instead of using them as crisp events, the author defined the empty area as the fuzzy set *EMP* and the occupied area as the fuzzy set *OBS*. That is, a fuzzy set *EMP* indicates that the sensor says here is free space and a fuzzy set *OBS* indicates the sensor says here is an obstacle.

Under the situation of obstacle and no noise in a sensor, $\{A_O\}$, of obstacle and noise in a sensor, $\{A_O, A_N\}$, and of free space and noise in a sensor, $\{A_F, A_N\}$, a sensor would say here is obstacle. The set $\{\{A_O\}, \{A_O, A_N\}, \{A_F, A_N\}\}$ is selected out of subsets of X and defined as a core of a fuzzy set *OBS*. Under the situation of free space and no noise in sensor, $\{A_F\}$, of obstacle and noise in a sensor, $\{A_O, A_N\}$, and of free space and noise in a sensor, $\{A_F, A_N\}$, a sensor would say here is free space. The set $\{\{A_F\}, \{A_O, A_N\}, \{A_F, A_N\}\}$ is selected out of subsets of X and defined as a core of a fuzzy set *EMP*. Therefore, fuzzy sets *OBS* and *EMP* are expressed as

$$\begin{aligned} OBS &= \{(x, \mu_{OBS}(x)), x \in X\} \\ &= \mu_{OBS}(\{A_O\})/\{A_O\} + \mu_{OBS}(\{A_F\})/\{A_F\} + \mu_{OBS}(\{A_O, A_N\})/\{A_O, A_N\} + \\ &\quad \mu_{OBS}(\{A_F, A_N\})/\{A_F, A_N\} \end{aligned} \tag{5.2}$$

where

$\mu_{OBS}(\{A_O\})$: The grade of membership for a situation of obstacle and no noise in a sensor when a sensor says obstacle area

$\mu_{OBS}(\{A_F\})$: The grade of membership for a situation of free space and no noise in a sensor when a sensor says obstacle area

$\mu_{OBS}(\{A_O, A_N\})$: The grade of membership for a situation of obstacle and noise in a sensor when a sensor says obstacle area

$\mu_{OBS}(\{A_F, A_N\})$: The grade of membership for a situation free space and noise in a sensor when a sensor says obstacle area

and

$$EMP = \{(x, \mu_{EMP}(x)), x \in X\}$$
$$= \mu_{EMP}(\{A_O\})/\{A_O\} + \mu_{EMP}(\{A_F\})/\{A_F\} + \mu_{EMP}(\{A_O, A_N\})/\{A_O, A_N\} +$$
$$\mu_{EMP}(\{A_F, A_N\})/\{A_F, A_N\} \quad (5.3)$$

where

$\mu_{EMP}(\{A_O\})$: The grade of membership for a situation of obstacle and no noise in a sensor when a sensor says free space area

$\mu_{EMP}(\{A_F\})$: The grade of membership for a situation of free space and no noise in a sensor when a sensor says free space area

$\mu_{EMP}(\{A_O, A_N\})$: The grade of membership for a situation of obstacle and noise in a sensor when a sensor says free space area

$\mu_{EMP}(\{A_F, A_N\})$: The grade of membership for a situation free space and noise in a sensor when a sensor says free space area

The process of determining values for degree of membership is a subjective process and it is not always necessary to obtain exact values for the degree of membership. A slight degree of error in the degree of membership will be less consequential than when a crisp event has an all-or-nothing representation. Instead of a mathematical approximation of the geometry of the beam, the author chose an approach of fuzzy sets constructed from statistical data. Even though this approach is not optimal to find values for degree of membership, it is a good approach to estimate and produce values for range sensors. The values are defined as a frequency distribution by collecting imprecise data.

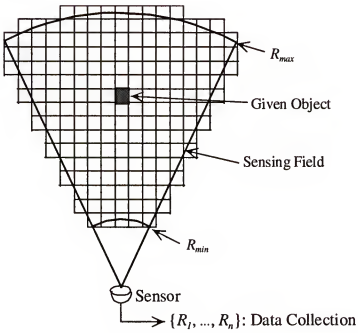

Figure 5-2 Tessellated Sensing Field

A sensor field is tessellated as a local grid map as shown Figure 5-2. By giving an object which is located at the distance R from a sensor and in a cell (i, j), a set of data, $\{R_1, \ldots R_n\}$ is collected and values for degree of membership are defined as follows.

$$\mu_{OBS}(\{A_O\}) = \frac{\text{Number of signals satisfying} \mid R_i - R \leq \varepsilon}{\text{Total number of samples}} \tag{5.4}$$

$$\mu_{EMP}(\{A_O, A_N\}) = \frac{\text{Number of no data and signals satisfying } R_i - R > \varepsilon}{\text{Total number of samples}} \tag{5.5}$$

Using information of free space between a sensor and an obstacle,

$$\mu_{EMP}(\{A_F, A_N\}) = \frac{\text{Number of signals satisfying } R_i - R > \varepsilon}{\text{Total number of samples}} \tag{5.6}$$

By removing an object from a sensing field,

$$\mu_{EMP}(\{A_F\}) = \frac{\text{Number of no data}}{\text{Total number of samples}} \tag{5.7}$$

$$\mu_{OBS}(\{A_F, A_N\}) = \frac{\text{Number of false signals}}{\text{Total number of samples}} \tag{5.8}$$

These values are distributed all over a sensing field because of the randomness of noise. 0.0 is assigned to $\mu_{OBS}(\{A_F\})$ and $\mu_{EMP}(\{A_O\})$ because a sensor returns a true signal under the situation of no noise. It is not possible to define $\mu_{OBS}(\{A_O, A_N\})$, because noise can not be measured as long as a sensor returns a true signal.

Fuzzy sets *OBS* and *EMP* obtained by the way discussed above are stored as a sensor database. A sensing field is defined by the characteristics of a range sensor. Each cell has two fuzzy sets, *OBS* and *EMP*, whose values for degree of membership are obtained experimentally during calibration.

When a sensor has a reading, the fuzzy distribution shown in Figure 5-3 is generated. Cells in the obstacle area have a fuzzy set *OBS* and cells in free space have a fuzzy set *EMP*. When a sensor has no reading, the fuzzy distribution shown in Figure5-3 is generated. All cells in the sensing area have a fuzzy set *EMP*.

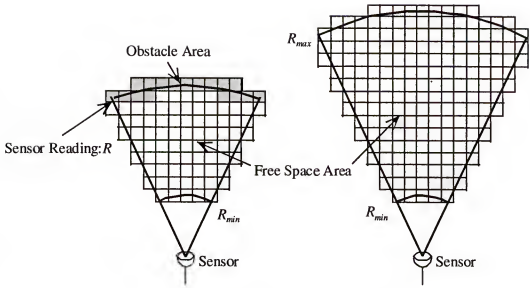

Figure 5-3 Fuzzy Distribution

After producing a fuzzy distribution, a fuzzy set is projected onto the local grid map and is given to a cell as input. As notations, a fuzzy set *OBS* after a transformation from a sensor coordinate system to a local grid map coordinate system is expressed as *OBS*(x,y) where x and y are the position of a cell in a local grid map coordinate system different from X and Y in the global coordinate system used in chapter 4.

Nonhomogeneous Markov Chain Approach

In the previous section, fuzzy modeling is discussed to represent the uncertainty such as randomness caused by noise and fuzziness caused by poor performance of sensors. A set of observations arranged chronologically is called a time series. The basic idea of the statistical theory of analysis of a time series is to regard the time series as an observation made on a family of random variables; that is, for each time, the observation is an observed value of a random variable. A family of random variables is called a stochastic process[Hoe72, Par62]. Regarding a sequence of fuzzy sets as a time series, the

nonhomogeneous Markov chain is applied to the stochastic process using a fuzzy model to reduce uncertainty.

The set of distinct values assumed by a stochastic process is called the state space. For a local grid map management, two states in an environment are considered and the state space is defined as $\{\{A_O\}, \{A_F\}\}$ in an environment for a vehicle. The state space of a stochastic process is countable and finite and the process can be called a chain.

A stochastic process that satisfies the following three restrictions are called a discrete-time Markov chain[Isa76, Dav91]. The first restriction is that the process be a discrete-time process. The second is that only processes that have a countable or finite state space. The final restriction is that the process satisfies the Markov property that given the present state, the past states have no influence on the future.

Definition 5-2

A stochastic process $\{X_k\}$, $k=1,2,\ldots$ with state space $S=\{1,2,3,\ldots\}$ is said to satisfy the Markov property if for every n and all states $i_1, i_2, \ldots, i_n$ it is true that

$$P[X_n=i_n \mid X_{n-1}=i_{n-1}, X_{n-2}=i_{n-2},\ldots, X_1=i_1] = P[X_n=i_n \mid X_{n-1}=i_{n-1}]$$

The movement of the process for the probability of occupancy among the states of the state space is determined by conditional probabilities. Different from a conditional probability in Bayes's theorem that produced $P(R \mid \{A_O\})$ from range sensor directly as a crisp event, the following conditional probabilities are defined as transition probabilities for the chain using fuzzy sets, *OBS* and *EMP*. The probability of $X_{n+1} = \{A_O\}$ given the occurrence of $X_n = \{A_O\}$ is defined as

$$P(X_{n+1} = \{A_O\} \mid X_n = \{A_O\}) = \max[P(X_n = \{A_O\}), \mu_{OBS}(\{A_O\})\cdot\min(\frac{n_{OBS}}{n}, m(n_{OBS})),$$

$$\mu_{OBS}(\{A_O, A_N\})\cdot\min(\frac{n_{OBS}}{n}, m(n_{OBS})), \mu_{EMP}(\{A_O, A_N\})\cdot\min(\frac{n_{EMP}}{n}, m(n_{EMP}))] \quad (5.9)$$

and, the probability of $X_{n+1} = \{A_F\}$ given the occurrence of $X_n = \{A_F\}$ is defined as

$$P(X_{n+1} = \{A_F\} \mid X_n = \{A_F\}) = \max[P(X_n = \{A_F\}), \mu_{OBS}(\{A_F, A_N\})\cdot\min(\frac{n_{OBS}}{n}, m(n_{OBS})),$$

$$\mu_{EMP}(\{A_F\})\cdot\min(\frac{n_{EMP}}{n}, m(n_{EMP})), \mu_{EMP}(\{A_F, A_N\})\cdot\min(\frac{n_{EMP}}{n}, m(n_{EMP}))] \quad (5.10)$$

where n_{OBS}: the number of the sequence of *OBS* from sensor modeling

n_{EMP}: the number of the sequence of *EMP* from sensor modeling

n: the total number of fuzzy sets, that is $n = n_{OBS} + n_{EMP}$

$m(\cdot)$: the weight at the initial stage of sequence

$P(X_{n+1} = \{A_O\} \mid X_n = \{A_O\})$ is the maximum value of four values. $P(X_n = \{A_O\})$ is the previous probability of occupancy in a cell. $\mu_{OBS}(\{A_O\})$, $\mu_{OBS}(\{A_O, A_N\})$ and $\mu_{EMP}(\{A_O, A_N\})$ are produced by fuzzy modeling for each sensing and these values indicate the degree of membership belonging to a state $\{A_O\}$in an environment. As introduced in the previous section, the sensor model is constructed in a stationary situation, while sensing is conducted under a dynamic situation. Obviously, those values are changed increasing the influence of obstacle-environment interaction. To extend to a dynamic situation that a vehicle is moving, weights of a relative frequency that increase with the repeatability are multiplied as compensation. The weight will be close to 1.0 if the sensor has many repeated answers, reflecting on the concept that repeatability reduces

uncertainty. To avoid 1.0 of relative frequency for the first couple of data, a minimum operation is used with $m(\cdot)$.

Similarly, $P(X_{n+1} = \{A_F\} \mid X_n = \{A_F\})$ is the maximum value of four values. $P(X_n = \{A_F\})$ is the previous probability of emptiness in a cell. $\mu_{EMP}(\{A_F\})$, $\mu_{OBS}(\{A_F, A_N\})$ and $\mu_{EMP}(\{A_F, A_N\})$ are produced by fuzzy modeling each sensing and these values indicate degree of membership belonging to a state $\{A_F\}$ in an environment. To extend to a dynamic situation, weights of a relative frequency that increase with much repeatability are multiplied as compensation.

Definition 5-3

A discrete-time Markov chain is said to be stationary or homogeneous in time if the probability of going from one state to another is independent of the time at which the step is being made. That is for all states i and j,

$$P[X_n = j \mid X_{n-1} = i] = P[X_{n+k} = j \mid X_{n+k-1} = i]$$

For $k = -(n-1), -(n-2), \ldots, -1, 0, 1, 2, \ldots$ the Markov chain is said to be nonstationary or nonhomogeneous if the condition for stationary fails.

Obviously, degrees of memberships are changed while a vehicle is moving. Therefore, the proposed Markov chain is nonhomogeneous and its formula is

$$\begin{cases} P(X_{n+1} = \{A_O\}) = P(X_n = \{A_O\}) \cdot P(X_{n+1} = \{A_O\} \mid X_n = \{A_O\}) + \\ \qquad\qquad P(X_n = \{A_F\}) \cdot P(X_{n+1} = \{A_O\} \mid X_n = \{A_F\}) \\ P(X_{n+1} = \{A_F\} = 1 - P(X_{n+1} = \{A_O\}) \end{cases} \tag{5.11}$$

A nonhomogeneous Markov chain is completely described by a starting vector and a sequence of transition matrices. A starting vector is the initial distribution of probabilities of the Markov chain and is defined as $\pi_0 = (P(X_0 = \{A_O\}), P(X_0 = \{A_F\}))$. For

map building, the cell where a vehicle has never been is initialized as unknown that is $\pi_0=(P(X_0 = \{A_O\}) = 0.5, P(X_0 = \{A_F\}) = 0.5)$, or the cell where a vehicle has been is initialized by a previous probability that is more than 0.5 when the cell is occupied and is less than 0.5 when the cell is empty. The transition matrix consists of conditional probabilities, contains all the relevant information regarding the movement of the process among the states in state space, and is defined as

$$P_n = \begin{bmatrix} P(X_{n+1} = \{A_O\} \mid X_n = \{A_O\}) & 1 - P(X_{n+1} = \{A_O\} \mid X_n = \{A_O\}) \\ 1 - P(X_{n+1} = \{A_F\} \mid X_n = \{A_F\}) & P(X_{n+1} = \{A_F\} \mid X_n = \{A_F\}) \end{bmatrix}. \quad (5.12)$$

A notation, $\pi^{(k)} = \pi_0 \cdot P_1 \cdot P_2 \cdot \ldots \cdot P_k$ and $\pi^{(m,k)} = \pi_0 \cdot P_{m+1} \cdot P_{m+2} \cdot \ldots \cdot P_k$. When γ_0 is the starting vector, similarly $\gamma^{(k)}$ and $\gamma^{(m,k)}$ will be used.

To see the behavior of the formula, whether a limiting vector is independent of choice of starting vector is verified through the ergodicity of the nonhomogeneous Markov chain. There is a weak ergodicity and a strong ergodicity. When a limiting vector is independent of the starting vector, the effect of the starting vector is lost after a long time. This is called a loss of memory. For a strong ergodicity, the behavior of the process is convergence and loss of memory. A weak ergodicity is the behavior that is loss of memory without convergence. A weak ergodicity will be used to prove strong ergodicity. When the formula has strong ergodicity, the limiting probability of obstacles is independent of the initial probability of a cell. That is, even though the vehicle approaches to obstacles in a different way and at a different time, the final probability must be the same value as long as a same sensor database is used. Therefore, it is possible that certainty can be increased after the vehicle comes back to the previous place when the first sensing is poor because of a long relative distance between the vehicle and the

obstacle. The remainder of this chapter will prove the strong ergodicity for the update formula.

A nonhomogeneous Markov chain is called weakly ergodic if for all m,

$$\lim_{k\to\infty} \sup_{\pi_0,\gamma_0} \| \pi^{(m,k)} - \gamma^{(m,k)} \| = 0 \tag{5.13}$$

where $\| \cdot \|$ is a norm with the meaning determined by whether there is a vector or a matrix inside the double bars,

$$\| \mathbf{f} \| = \sum_{i=1}^{\infty} | f_i | \text{ if } \mathbf{f} \text{ is a vector}$$

$$\| \mathbf{A} \| = \sup_i \sum_{j=1}^{\infty} | a_{ij} | \text{ if } \mathbf{A} \text{ is a square matrix}$$

and is called strongly ergodic if there exists a vector $\mathbf{q} = (q_1, q_2, \ldots)$, with $\|\mathbf{q}\| = 1$ and $q_i \geq 0$, for $i = 1, 2, 3, \ldots$ such that for all m

$$\lim_{k\to\infty} \sup_{\pi_0} \| \pi^{(m,k)} - \mathbf{q} \| = 0 . \tag{5.14}$$

It is difficult to show that a chain is weakly or strongly ergodic by using the definition directly. Instead, the ergodic coefficient can be used to give characterization of weak and strong ergodicity. The ergodic coefficient is defined as follows.

Definition 5-4

Let P be a stochastic matrix. The ergodic coefficient of P denoted by $\alpha(P)$ is defined by

$$\alpha(P) = 1 - \sup_{i,k} \sum_{j=1}^{\infty} \max(0, p_{ij} - p_{kj}) = \inf_{i,k} \sum_{j=1}^{\infty} \min(p_{ij}, p_{kj}) . \tag{5.15}$$

The formula can be determined whether a nonhomogeneous Markov chain is weakly ergodic with the following theorem.

Theorem 5-1

Let $\{X_n\}$ be a nonhomogeneous Markov chain with transition matrices $\{P_n\}_{n=1}^{\infty}$ The chain $\{X_n\}$ is weakly ergodic if and only if there exists a subdivision of $P_1 \cdot P_2 \cdot P_3 \cdots$ into blocks of matrices $[P_1 \cdot P_2 \cdots P_{n1}] \cdot [P_{n1+1} \cdot P_{n1+2} \cdots P_{n2}] \cdots [P_{nj+1} \cdot P_{nj+2} \cdots P_{n(j+1)}] \cdots$ such that

$$\sum_{j=0}^{\infty} \alpha(P^{(n_j, n(j+1))}) = \infty \tag{5.16}$$

where $n_0 = 0$.

For the formula, let each P_i, $i = 1,2,\ldots$, be blocks of matrices then

$$\sum_{j=0}^{\infty} \alpha(P) = \sum_{j=0}^{\infty} \{(\min(P(X_{n+1} = \{A_O\} \mid X_n = \{A_O\}), 1 - P(X_{n+1} = \{A_F\} \mid X_n = \{A_F\})) + \min(P(X_{n+1} = \{A_F\} \mid X_n = \{A_F\}), 1 - P(X_{n+1} = \{A_O\} \mid X_n = \{A_O\}))\}. \tag{5.17}$$

Assume that $\sum_{j=0}^{\infty} \alpha(P) < \infty$. According to the theorem of divergence, the only way $\sum_{j=0}^{\infty} \alpha(P)$ is finite is if both $P(X_{n+1} = \{A_O\} \mid X_n = \{A_O\})$ and $P(X_{n+1} = \{A_F\} \mid X_n = \{A_F\})$ are close to 1.0. To look into values of them, the behavior of components in a maximum operation are needed to verify. $P(X_n = \{A_O\})$ in $P(X_{n+1} = \{A_O\} \mid X_n = \{A_O\})$ and $P(X_n = \{A_F\})$ in $P(X_{n+1} = \{A_F\} \mid X_n = \{A_F\})$ are complementary to each other, that is $P(X_n = \{A_O\}) = 1.0 - P(X_n = \{A_F\})$. So, it is not possible that both of them are close to 1.0. When $P(X_n = \{A_O\})$ is close to 1.0, a cell has a high confidence of occupancy and sensor would

have a high repeatability of fuzzy set *OBS*. Then, increasing a relative frequency, $\frac{n_{OBS}}{n}$, max $[\mu_{OBS}(\{A_O\})\cdot\min(\frac{n_{OBS}}{n}, m(n_{OBS})), \mu_{OBS}(\{A_O, A_N\})\cdot\min(\frac{n_{OBS}}{n}, m(n_{OBS})), \mu_{EMP}(\{A_O, A_N\})\cdot\min(\frac{n_{EMP}}{n}, m(n_{EMP}))]$ whose values are dependent on sensor model has a higher probability than $\max[\mu_{OBS}(\{A_F, A_N\})\cdot\min(\frac{n_{OBS}}{n}, m(n_{OBS})), \mu_{EMP}(\{A_F\})\cdot\min(\frac{n_{EMP}}{n}, m(n_{EMP})), \mu_{EMP}(\{A_F, A_N\})\cdot\min(\frac{n_{EMP}}{n}, m(n_{EMP}))]$. Hence, when $P(X_{n+1} = \{A_O\} \mid X_n = \{A_O\})$ is close to 1.0, $P(X_{n+1} = \{A_F\} \mid X_n = \{A_F\})$ can not be close to 1.0. Similarly, when $P(X_n = \{A_F\})$ is close to 1.0, a cell has a high confidence of emptiness and sensor would have a high repeatability of fuzzy set *EMP*. Then, increasing a relative frequency, $\frac{n_{EMP}}{n}$, $\max[\mu_{OBS}(\{A_O\})\cdot\min(\frac{n_{OBS}}{n}, m(n_{OBS})), \mu_{OBS}(\{A_O, A_N\})\cdot\min(\frac{n_{OBS}}{n}, m(n_{OBS})), \mu_{EMP}(\{A_O, A_N\})\cdot\min(\frac{n_{EMP}}{n}, m(n_{EMP}))]$ has a lower probability than $\max[\mu_{OBS}(\{A_F, A_N\})\cdot\min(\frac{n_{OBS}}{n}, m(n_{OBS})), \mu_{EMP}(\{A_F\})\cdot\min(\frac{n_{EMP}}{n}, m(n_{EMP})), \mu_{EMP}(\{A_F, A_N\})\cdot\min(\frac{n_{EMP}}{n}, m(n_{EMP}))]$. Hence, when $P(X_{n+1} = \{A_F\} \mid X_n = \{A_F\})$ is close to 1.0, $P(X_{n+1} = \{A_O\} \mid X_n = \{A_O\})$ can not be close to 1.0. Therefore, both $P(X_{n+1} = \{A_O\} \mid X_n = \{A_O\})$ and $P(X_{n+1} = \{A_F\} \mid X_n = \{A_F\})$ can not be close to 1.0 at any situation. By contradiction, $\sum_{j=0}^{\infty} \alpha(P) = \infty$ and the formula is weakly ergodic.

For a strong ergodicity, the proof is done using the following theorem.

Theorem 5-2

Let $\{P_n\}$ be a sequence of transition matrices corresponding to a nonhomogeneous Markov chain with $P_n \in \mathscr{P}$. If $\| P_n - P \| \to 0$ as $n \to \infty$ where P is weakly ergodic, then the chain is strong ergodic.

As discussed about the proof of weak ergodicity, when a cell is occupied by an obstacle, the conditional probability $P(X_{n+1} = \{A_O\} \mid X_n = \{A_O\})$ is getting bigger with a higher confidence of $P(X_n = \{A_O\})$ and $P(X_{n+1} = \{A_F\} \mid X_n = \{A_F\})$ is getting smaller to reduce a contradiction of existence of an obstacle.

Let $\lim_{n\to\infty} P(X_{n+1} = \{A_O\} \mid X_n = \{A_O\})$ and $\lim_{n\to\infty} P(X_{n+1} = \{A_F\} \mid X_n = \{A_F\})$ be $\frac{1}{2} + \varepsilon$ and δ respectively, where $0.0 \le \varepsilon, \delta \le 0.5$, then

$$P = \lim_{n\to\infty} P_n = \begin{bmatrix} \frac{1}{2}+\varepsilon & \frac{1}{2}-\varepsilon \\ 1-\delta & \delta \end{bmatrix}. \tag{5.18}$$

The ergodic coefficient of P is

$$\alpha(P) = \min(\frac{1}{2}+\varepsilon, 1-\delta) + \min(\frac{1}{2}-\varepsilon, \delta). \tag{5.19}$$

Taking a summation of $\alpha(P)$ from 0 to ∞,

$$\sum_{j=0}^{\infty} \alpha(P) = \sum_{j=0}^{\infty} \{\min(\frac{1}{2}+\varepsilon, 1-\delta) + \min(\frac{1}{2}-\varepsilon, \delta)\} = \infty, \tag{5.20}$$

because of $\min(\frac{1}{2}+\varepsilon, 1-\delta) > 0.5$. Hence, P is weakly ergodic. Similarly, when a cell is free space, the conditional probability $P(X_{n+1} = \{A_F\} \mid X_n = \{A_F\})$ is getting bigger with a higher confidence of $P(X_n = \{A_F\})$ and $P(X_{n+1} = \{A_O\} \mid X_n = \{A_O\})$ is getting smaller to reduce a contradiction of existence of an obstacle.

Let $\lim_{n\to\infty} P(X_{n+1}=\{Ao\} \mid X_n=\{Ao\})$ and $\lim_{n\to\infty} P(X_{n+1}=\{A_F\} \mid X_n=\{A_F\})$ be ε and $\frac{1}{2}+\delta$ respectively, where $0.0 \le \varepsilon, \delta \le 0.5$, then

$$P = \lim_{n\to\infty} P_n = \begin{bmatrix} \varepsilon & 1-\varepsilon \\ \frac{1}{2}-\delta & \frac{1}{2}+\delta \end{bmatrix}. \tag{5.20}$$

The ergodic coefficient of P is

$$\alpha(P) = \min(\varepsilon, \frac{1}{2}-\delta) + \min(1-\varepsilon, \frac{1}{2}+\delta). \tag{5.21}$$

Taking a summation of $\alpha(P)$ from 0 to ∞,

$$\sum_{j=0}^{\infty} \alpha(P) = \sum_{j=0}^{\infty} \{\min(\varepsilon, \frac{1}{2}-\delta) + \min(1-\varepsilon, \frac{1}{2}+\delta)\} = \infty, \tag{5.22}$$

because of $\min(1-\varepsilon, \frac{1}{2}+\delta) > 0.5$. Hence, P is weakly ergodic. Therefore, the formula of the chain is strongly ergodic.

This strong ergodicity indicates the limiting probability value in a cell is the independent of the initial probability. In an outdoor operation such as an exploration, a vehicle approaches to obstacles in a different way and at a different time, and also some obstacles maybe disappear or come out. However, this formula is possible that certainty can be increased after the vehicle returns to the previously visited location according to the status of the environment.

CHAPTER 6
GLOBAL CONTOUR MAP UPDATE

As a vehicle is moving in an outside field, a local grid map that has a limited size is also moving with the step of a resolution of grid mesh. Cell values that indicate a probability of an obstacle come out of the local grid map. To store them into a global map, they are converted to a global coordinate system with a transformation from the grid model to a boundary representation that is a probability contour of the obstacle. In this chapter, a datum that comes out from a local grid cell is considered as a prime element, a bubble. Two bubbles are fused into a bigger bubble, that is a polygon. A bigger bubble absorbs a bubble and increases a size of a bubble. Moreover, a bigger bubble and a bigger bubble are fused with each other through a shared bubble. When a vehicle returns to a previous place, the local grid map is initialized using the previous polygonal contour map. In this chapter, how this is all accomplished is described in detail.

Linked List for Polygonal Contour

To represent a polygonal contour map, the author applied a two dimensional linked list that consists of a polygon linked list and a vertex linked list for each polygon. Each group of probabilities has it own linked list. A polygon linked list has polygon nodes and a vertex link list has vertex nodes, as shown in Figure 6-1.

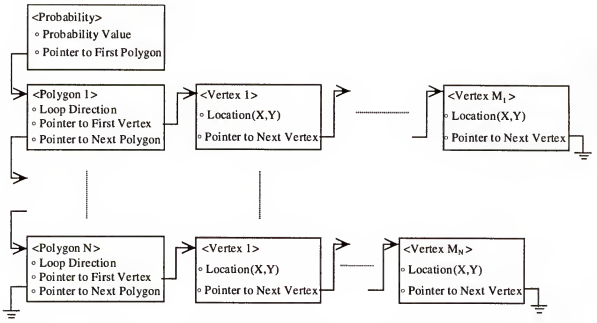

Figure 6-1 Two Dimensional Linked List for Polygonal Contour

Polygon nodes have attributions such as a loop direction, a pointer to the next polygon and a pointer to a first vertex. When there is no next polygon, the pointer is set to null. For a polygon list, there are two operations to maintain the list, that is addition and deletion. To add a polygon node, the size of the node is allocated in memory and the node is added to the end of the polygon linked list setting attribute values. To delete a polygon node, the node is freed from a polygon link and memory and a new linkage between nodes is established.

Vertex nodes have attributions such as values of X and Y in a global coordinate system and a pointer to the next vertex. The order of the vertex nodes is defined as a counterclockwise fashion for an area inside a polygon and as a clockwise fashion for an area outside a polygon. The next pointer at the end of the vertex list is set to null. To maintain a vertex linked list, there are three operations, that is addition, deletion and insertion. Different from a polygon linked list, insertion is used to absorb a bubble to a

polygon. To add a vertex node, the size of the node is allocated in memory and the node is added to the end of the vertex linked list setting attribute values. To delete a vertex node, the node is freed from the list and a new linkage between nodes is established. To insert a vertex node, the size of the node is allocated in memory and the node is inserted in front of the indicated node.

Description of a Bubble

A cell coming out of a local grid map is called as a bubble and each vertex in a bubble is numbered in a counterclockwise fashion starting from a upper right vertex and a direction of sides is also counterclockwise as shown in Figure 6-2.

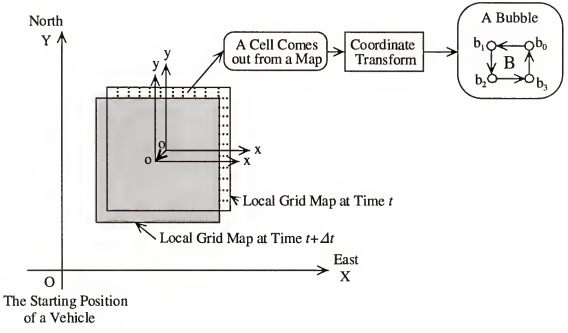

Figure 6-2 Bubble Generation

A cell (x, y) in a local coordinate system is transformed to a global coordinate system by

$$\begin{cases} X = \{x + (\text{round})(\dfrac{\text{X position of a vehicle}}{\text{Grid resolution}})\} \times (\text{Grid resolution}) \\ Y = \{y + (\text{round})(\dfrac{\text{Y position of a vehicle}}{\text{Grid resolution}})\} \times (\text{Grid resolution}) \end{cases} \quad (6.1)$$

Each position of four vertices in a bubble is expressed as

$$(X_{b0}, Y_{b0}) = (X + (\text{Grid resolution})/2,\ Y + (\text{Grid resolution})/2) \quad (6.2)$$

$$(X_{b1}, Y_{b1}) = (X - (\text{Grid resolution})/2,\ Y + (\text{Grid resolution})/2) \quad (6.3)$$

$$(X_{b2}, Y_{b2}) = (X - (\text{Grid resolution})/2,\ Y - (\text{Grid resolution})/2) \quad (6.4)$$

$$(X_{b3}, Y_{b3}) = (X + (\text{Grid resolution})/2,\ Y - (\text{Grid resolution})/2). \quad (6.5)$$

A bubble is then verified whether it is inside an area defined by other polygons or not. Each side is projected onto its closest side of a polygon. When a direction of the polygon is counterclockwise, if all directions of sides of a bubble are matched with directions of sides of a polygon, the bubble is located inside the polygon. Otherwise, the bubble is outside the polygon. When a direction of the polygon is clockwise, if all directions of sides of a bubble are opposite to directions of sides of a polygon, the bubble is located outside the polygon. Otherwise, the bubble is inside the polygon. Naturally, areas defined by polygons are closed and clockwise polygons have their own pair of counterclockwise polygons.

When it is inside a polygon, the bubble is eliminated. When it is outside a polygon, the following data structure is produced checking connectivity with a polygon.

match_count: number of matched vertices between a bubble and a polygon

match_polygon: Pointer of a matched polygon

match_bvertex[*i*]: *ith* matched vertex number of a bubble

match_pvertex[*i*]: *ith* matched vertex node pointer of a polygon

online_count: number of online vertices in a bubble

online_polygon: Pointer of a polygon whose side has a vertex of a bubble

online_bvertex[*i*]: *ith* online vertex number of a bubble

online_pvertex[*i*][0]: pointer of *ith* start vertex of an onlined side of a polygon

online_pvertex[*i*][1]: pointer of *ith* end vertex of an onlined side of a polygon

When a bubble has no connectivity with any other polygons, a bubble is regarded as a polygon and added a new polygon node to a link list. When a bubble has some connectivity with a polygon, then a bubble is fused into a polygon following fusion rules described in next section.

Fusion Rules

Using information of connectivity between a bubble and a polygon, those are fused into a polygon by the following rules. In a rule, a left side indicates the if-clause and a right side indicates the then-clause. Four circles represent the vertices of a bubble and rectangles represent the vertices of a polygon. Arrows indicate the direction of a polygon. The bubble vertex that is any connection with a vertex in a polygon is called as a free bubble vertex. The bubble vertex that is matched with a vertex in a polygon is called a matched bubble vertex. The bubble vertex that is on a side of a polygon is called an online bubble vertex. Symmetric patterns are omitted to list up in fusion rules.

Rule 1: All four vertices of a bubble are inserted into a polygon.

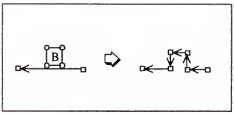

Rule 2: A bubble creates two new polygons using vertices of a bubble.

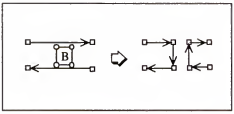

Rule 3: Two free bubble vertices and one online bubble vertex are inserted into a polygon.

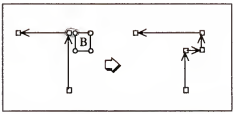

Rule 4: One free bubble vertex two online bubble vertices are inserted in to a polygon.

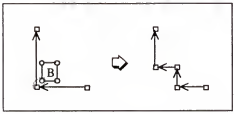

Rule 5: All four vertices of a bubble are inserted into a polygon.

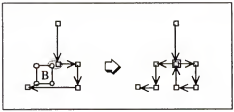

Rule 6: A bubble creates two new polygons using vertices of a bubble.

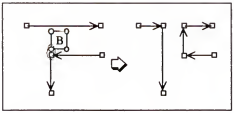

Rule 7: Two matched polygon vertices are replaced with two free bubble vertices.

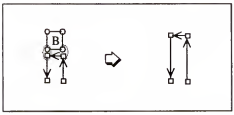

Rule 8: Two matched polygon vertices are replaced with one free bubble vertex and one online bubble vertex.

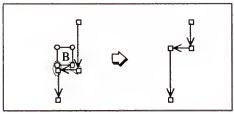

Rule 9: Two matched polygon vertices are replaced with two online bubble vertices.

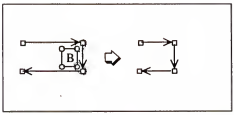

Rule 10: One matched polygon vertex is replaced with a free bubble vertex and one online bubble vertex and another matched bubble vertex are inserted.

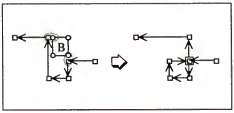

Rule 11: One matched polygon vertex is replaced with another matched bubble vertex and a free bubble vertex and an online bubble vertex are inserted.

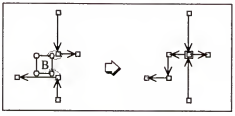

Rule 12: One matched polygon vertex is replaced with one online bubble vertex and another matched bubble vertex and another online vertex are inserted.

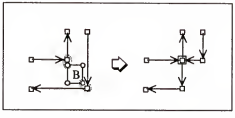

Rule 13: A bubble creates two new polygons using vertices of a bubble.

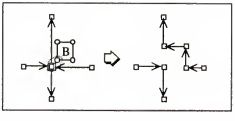

Rule 14: A bubble creates two new polygons using vertices of a bubble.

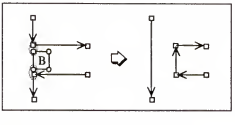

Rule 15: A bubble creates two new polygons using vertices of a bubble.

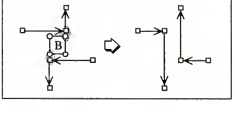

Rule 16: A bubble creates two new polygons using vertices of a bubble.

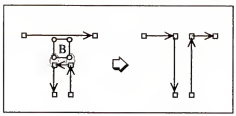

Rule 17: All four vertices of a bubble are inserted into a polygon.

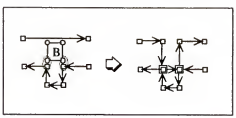

Rule 18: One matched polygon vertex is replaced with another matched bubble vertex and a free bubble vertex and an online bubble vertex are inserted.

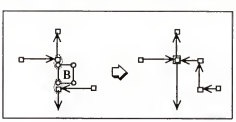

Rule 19: Three matched polygon vertices are replaced with one free bubble vertex.

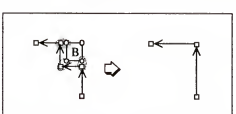

Rule 20: Three matched polygon vertices are replaced with one online bubble vertex.

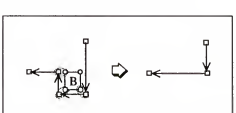

Rule 21: Two matched polygon vertices are replaced with one online bubble vertex and another matched bubble vertex.

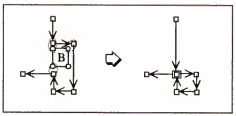

Rule 22: A bubble creates two new polygons using vertices of a bubble.

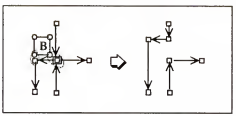

Rule 23: Two matched polygon vertices are replaced with one free bubble vertex and another matched bubble vertex.

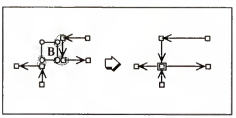

Rule 24: Two matched polygon vertices are replaced with one online bubble vertex and another matched bubble vertex.

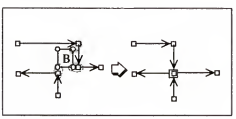

Rule 25: A bubble creates two new polygons using vertices of a bubble.

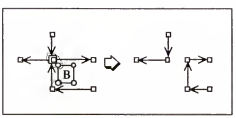

Rule 26: A bubble creates two new polygons using vertices of a bubble.

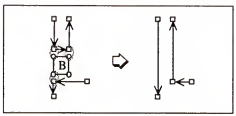

Rule 27: Three bubble vertices are inserted and one matched polygon vertex is deleted.

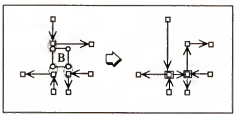

Rule 28: A bubble creates two new polygons using vertices of a bubble.

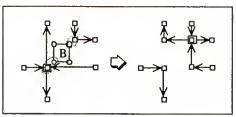

Rule 29: Four matched polygon vertices are deleted.

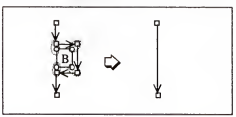

Rule 30: A polygon is deleted.

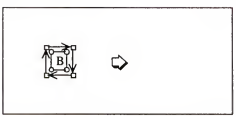

Rule 31: Three consecutive matched polygon vertices are replaced with another matched bubble vertex.

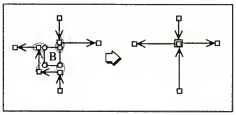

Rule 32: A bubble creates two new polygons using vertices of a bubble.

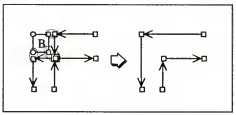

Rule 33: A bubble creates two new polygons using vertices of a bubble.

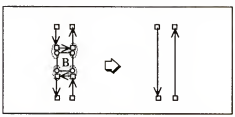

Rule 34: A bubble creates two new polygons using vertices of a bubble.

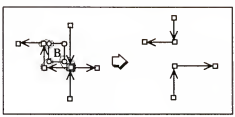

Rule 35: A bubble creates two new polygons using vertices of a bubble.

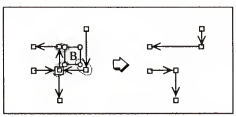

Rule 36: A bubble creates two new polygons using vertices of a bubble.

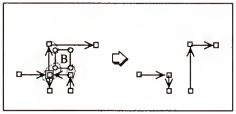

Rule 37: A bubble creates two new polygons using vertices of a bubble.

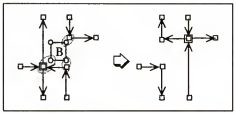

Rule 38: A bubble creates three new polygons using vertices of a bubble.

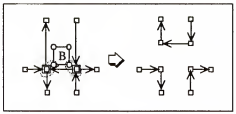

Rule 39: Four matched polygon vertices are deleted.

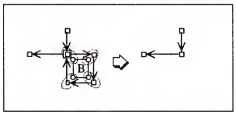

Rule 40: A bubble creates two new polygons using vertices of a bubble.

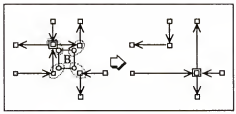

Rule 41: A bubble creates two new polygons using vertices of a bubble.

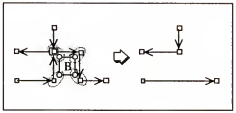

Rule 42: A bubble creates two new polygons using vertices of a bubble.

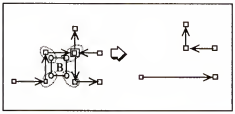

Rule 43: A bubble creates three new polygons using vertices of a bubble.

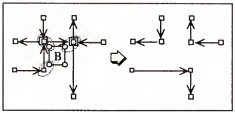

Rule 44: A bubble creates three new polygons using vertices of a bubble.

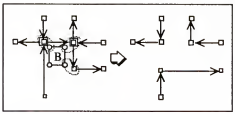

Rule 45: A bubble creates two new polygons using vertices of a bubble.

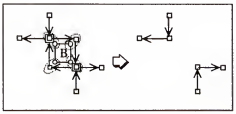

Rule 46: A bubble creates two new polygons using vertices of a bubble.

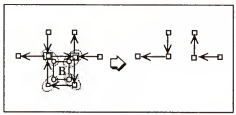

Rule 47: A bubble creates three new polygons using vertices of a bubble.

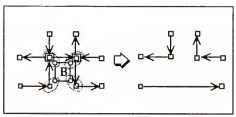

For a polygon and a polygon fusion, the shared bubble by both of polygons is used like glue. The procedure shown in Figure 6-3 is as follows.

1. Using a bubble two polygons to be fused are obtained.
2. Using a bubble the second polygon is changed to an open loop that will be inserted into a first polygon and one vertex in the first polygon is selected as a connecting point.
3. Inserting vertices of open loop into the first polygon between connecting points, new polygon is created. Overlapping vertex and side are checked and deleted from a new polygon.

Initialization of a Local Grid Map

While a vehicle is moving, new cells are generated in the local grid map and cells come out of the map. To initialize a value for a new cell, the cell is temporally regarded as a bubble. Verifying inside which probability area defined by polygons the bubble is, the value is set in the same manner as in the description of a bubble.

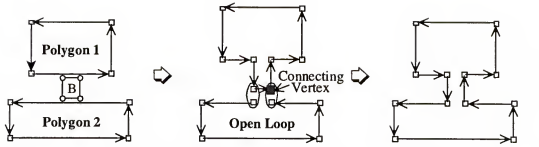

Step 1 Obtain Two Polygon that Share a Same Bubble

Step 2 Make Open Loop and Find Connecting Vertices

Step 3 Insert Open Loop and Check Consistency of Vertex Order

Figure 6-3 Polygon-Polygon Fusion

CHAPTER 7
RESULTS AND CONCLUSIONS

The map management strategies were developed and demonstrated in a simulation. In this chapter, some techniques used in the simulation are introduced. Grid model techniques discussed in chapter 4 are simulated and evaluated in an indoor environment, and are also investigated as a possibility for application in an outdoor environment. The nonhomogeneous Markov chain approach described in chapter 5 is also demonstrated in the simulation and is verified in the outdoor environment. All results from test runs of the simulation program are summarized at the end of this chapter. The chapter ends with some conclusions that can be drawn from this research.

Simulation

Simulation programs are written in C++ with Inventor[Wer94] and Motif[Bra92] used to develop the computer graphics and the graphic user interface. The dimension of the local grid map is 41×41 cells and each cell represents a real-world square of size $0.5 \times 0.5\ m^2$.

General range sensors are generated using a picking action in Inventor. The picking action finds objects along a ray from the camera through a point on the near plane of the viewing volume. The ray is specified by the coordinates of a window-space pixel. In the simulation, rays are distributed uniformly from 0° to 180° in front as shown Figure 7-1 and the number of rays can be changed. Uniform distributed noise is added to general

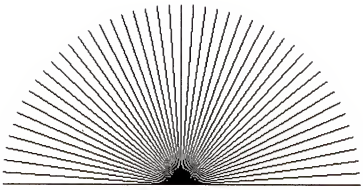

Figure 7-1 General Range Sensor

range sensors and produces two kinds of errors. One is an error in distance caused by the environment-obstacle interaction, and the other is a false detection caused by the sensor performance. The user can change the level of noise. Range data of ultrasonic sensors and of a laser range scanner are simulated by taking a minimum value of distance within each sensor field. A maximum distance, a minimum distance and angular resolution, specifies each sensor field. Each sensor is distributed uniformly from 0° to 180° in front using the specified number of sensors. Sensors can detect obstacles of sphere, cylinder, cone and box as generated by Inventor.

The car-like vehicle developed by Rankin[Ran97] is used in this simulation. It is assumed that no wheel slippage occurs and that no acceleration and deceleration are considered. To update the position and heading of the simulated vehicle, the following equations are used. For a three dimensional motion, elevation, pitch, and roll are calculated by using information of terrain where a vehicle is.

$$\theta_{new} = \theta_{old} + \mathrm{sgn}(\phi) \cdot \frac{v \cdot \Delta t \cdot \tan\phi}{W} \tag{7.1}$$

$$x_{new} = \begin{cases} x_{old} + \dfrac{W}{\tan\phi}\left(1 - \cos\left(\mathrm{sgn}(\phi) \cdot \dfrac{v \cdot \Delta t \cdot \tan\phi}{W}\right)\right) & \text{if } \phi \neq 0 \\ x_{old} + v \cdot \Delta t \cdot \cos\theta_{new} & \text{if } \phi = 0 \end{cases} \tag{7.2}$$

$$y_{new} = \begin{cases} y_{old} + \dfrac{W}{\tan\phi} \cdot \sin\left(\mathrm{sgn}(\phi) \cdot \dfrac{v \cdot \Delta t \cdot \tan\phi}{W}\right) & \text{if } \phi \neq 0 \\ y_{old} + v \cdot \Delta t \cdot \sin\theta_{new} & \text{if } \phi = 0 \end{cases} \tag{7.3}$$

where

W: Length of a vehicle ϕ: Steering angle v: Vehicle speed

Δt: Sampling time

The database for fuzzy modeling described in chapter 5 is constructed using a simulated ultrasonic sensor and a simulated laser range scanner.

To evaluate several update formula with sensor modeling as discussed in chapter 4 and the nonhomogeneous Markov chain with fuzzy modeling developed in chapter 5, the following environmental factors are changed, and the number of false detection and missing obstacles is used as a performance index.

1. Indoor situation, flat terrain, and rugged terrain.
2. Shape, size, and population density of obstacles.
3. Vehicle speed.
4. Laser range scanner, ultrasonic sensor, and both.
5. Noise.

The indoor situation uses the course shown in Figure 7-2 and each room has an obstacle that is located at the center of a room. Flat terrain in outdoor environment uses a course consisting of 29 different kinds of objects. The course is shown in Figure 7-3 and a description of the obstacles is shown in Table 7-2. Rugged terrain in an outdoor

environment uses the same course as in the case of flat terrain. However, a vehicle has a roll and a pitch based on the slope of terrain. The course is shown in Figure 7-3 and a description of obstacles is shown in Table 7-2.

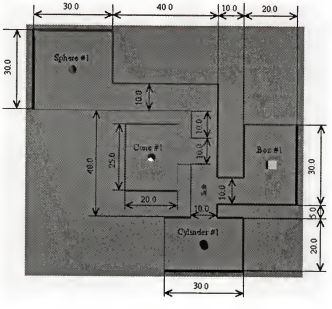

Figure 7-2 Indoor Environment

Table 7-1 Description of Obstacles in Indoor Environment

OBJECT	POSITION		SIZE		
	X	Y	S_x	S_y	S_z
Sphere #1	-50.0	45.0	3.0	3.0	3.0
Cone #1	-20.0	12.5	3.0	3.0	3.0
Box #1	25.0	10.0	3.0	3.0	3.0
Cylinder #1	0.0	-20.0	3.0	3.0	3.0

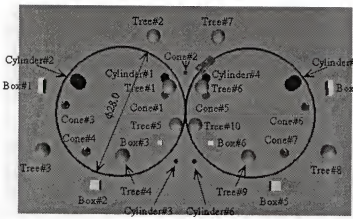

Figure 7-3 Outdoor Environment

Table 7-2 Description of Obstacles in Outdoor Environment

OBJECT	POSITION		SIZE		
	X	Y	S_x	S_y	S_z
Box #1	-31.5	5.0	1.0	3.0	2.0
Box #2	-19.0	-16.0	2.0	2.0	2.0
Box #3	-5.5	-7.0	1.0	1.0	1.0
Box #4	31.5	5.0	1.0	1.0	1.0
Box #5	19.0	-16.0	2.0	2.0	2.0
Box #6	5.5	-7.0	1.0	1.0	1.0
Cone #1	-4.5	3.5	2.0	2.0	2.0
Cone #2	0.0	8.5	1.0	1.0	2.0
Cone #3	-26.5	1.0	2.0	2.0	2.0
Cone #4	-21.5	-9.0	2.0	2.0	2.0
Cone #5	4.5	3.5	2.0	2.0	2.0
Cone #6	26.5	1.0	2.0	2.0	2.0
Cone #7	21.5	-9.0	2.0	2.0	2.0
Cylinder #1	-4.5	7.0	2.0	2.0	2.0
Cylinder #2	-23.5	6.0	3.0	3.0	3.0
Cylinder #3	-2.0	-11.0	1.0	1.0	1.0
Cylinder #4	4.5	7.0	2.0	2.0	2.0
Cylinder #5	23.5	6.0	3.0	3.0	3.0
Cylinder #6	2.0	-11.0	1.0	1.0	1.0

Table 7-2 (Continued)

OBJECT	POSITION		SIZE		
	X	Y	S_x	S_y	S_z
Tree #1 (Trunk part)	-3.5	4.5	0.7	0.7	5.0
Tree #2 (Trunk part)	-7.0	15.5	0.7	0.7	5.0
Tree #3 (Trunk part)	-29.5	-9.0	0.7	0.7	5.0
Tree #4 (Trunk part)	-13.0	-10.0	0.7	0.7	5.0
Tree #5 (Trunk part)	-2.0	-3.5	0.7	0.7	5.0
Tree #6 (Trunk part)	3.5	4.5	0.7	0.7	5.0
Tree #7 (Trunk part)	7.0	15.5	0.7	0.7	5.0
Tree #8 (Trunk part)	29.5	-9.0	0.7	0.7	5.0
Tree #9 (Trunk part)	13.0	-10.0	0.7	0.7	5.0
Tree#10 (Trunk part)	2.0	-3.5	0.7	0.7	5.0

The vehicle speeds are 0.83 m/s and 1.5 m/s. Zero and 20% are used as noise level for general range sensors. A ray of laser range scanner has a 0.5 ~ 10.0m range distance and the beam aperture is less than 1 degree. An ultrasonic sensor has a 0.5 ~ 6.0m range distance and beam aperture of 30 degrees.

The results are summarized from Figure 7-4 to Figure 7-136. In an indoor situation, each result shows the vehicle path on the left and the global contour map on the right. For an outdoor situation, only the global contour map is shown for each result. Red polygons in a global contour indicates more than 75% probability of occupancy, yellow ones are between 60% and 75%, black ones are between 0% and 15%, and blue ones are also between 0% and 15% and clockwise direction of polygon. Orange rectangle shows the scale $20.5 \times 20.5 m^2$.

Probability Theory Approach

The results obtained with the probability theory approach are shown from Figure 7-4 to Figure 7-27. In this simulation a 10% deviation error of the laser range scanner and ultrasonic sensor is used. Figure 7-5 and Figure 7-7 are well matched with the indoor experiment done by Maravec and Elfes, and indicates that probability in a cell reaches the limiting probability fast enough for 0.83 m/s and 1.5 m/s. The normalization in equation (4.8) works well to emphasize the obstacle information.

In the probability density function, the probability of occupancy becomes lower around the border of the sensing field but not zero. Hence, equation (4.8) lifts it to the higher value and the probability of occupancy in a cell located around the obstacle becomes higher. Hence, the resolution of obstacles is improved by using the laser range scanner that has a better performance than the ultrasonic sensors as shown in Figure 7-4 and Figure 7-6.

However, when a sensor has noise, the normalization works negatively. Data contaminated by noise are recognized as an obstacle and added to a previous map value, as seen in from Figure7-8 and Figure 7-11. Noise and poor performance of the sensor is lethal for the map in the probability theory approach. Therefore, it is not possible to apply this approach for the outdoor environment where more noise caused by obstacle-environment interaction is expected. The results shown in Figure 7-16 to 7-19 supports this.

Bayes's Theorem Approach

The results for Bayes's theorem approach are shown from Figure 7-28 to Figure 7-51. A 10% deviation error is used for the probabilistic sensor model. Figure 7-29 and Figure 7-31 are well matched with the indoor experiment done by Elfes and Matthies, and indicates that probability in a cell reaches the limiting probability fast enough for 0.83 m/s and 1.5 m/s. Bayes's theorem works well to emphasize the obstacle information.

In Bayes's theorem, there is one probability in a cell that is updated in every sensing. Even though a cell of free space around the detected obstacle has a probability of occupancy, the probability can be corrected by another sensing that gives the empty information to the cell. Hence, the resolution of obstacles is independent from sensor performance as shown in Figure 7-28 and Figure 7-30. Also this multiple detection reduces the noise influence. Figures 7-32 to Figure 7-35 shows the improvement of noise reduction compared with the probability theory approach. Bayes's theorem approach, that is very well known grid map update used in an indoor environment, is useful enough for the indoor environment with the conventional noise reduction technique.

However, when objects are spread out over the terrain, the repeatability of the detection decreases. When a sensor has noise, the probabilistic model whose maximum value is 1.0 is produced. Even though previous map has low probability of obstacles as free space, the updated probability becomes 1.0 as produced by noise. And, this updated probability is not changed until a new reading occurs. Therefore, this approach is very sensitive to noise and is not suitable for use in the outdoor environment as shown from Figure 7-40 to Figure 7-43.

Histogram Method Approach

The results for the histogram method approach are shown from Figure 7-52 to Figure 7-76. The value for increment is +3, the value for decrement is –1, and the maximum certainty value is 15 as Borenstein and Koren used in their indoor experiment. Figure 7-53 and Figure 7-55 are well matched with their experiment and indicates a multiple detection of obstacles is necessary for this approach to reach the limiting value. When a vehicle moves faster, the maximum value of occupancy in a cell becomes less. To distinguish obstacles, the threshold value can be changed. However, when the cell value of occupancy is not enough high, a low threshold also regards noise as an obstacle as shown from Figure 7-56 to Figure 7-59. In their experiment, the average speed of a vehicle is 0.58 m/s.

The resolution of obstacles is independent from sensors because the same simplified histogramic sensor model is used for every sensor as seen in Figure 7-52 and Figure 7-54. This approach is useful when a vehicle speed is slow enough to increase the quality of the map under the specific space where the threshold is constant. Therefore, this approach is too simplified to use in the outdoor environment.

Fuzzy Logic Approach

The results for the fuzzy logic theorem approach are shown from Figure 7-77 to Figure 7-100. The deviation error of sensors is 0.5 m. $h_1 = 1.2$, $h_2 = 1$, and $h_3 = 0.1$ for the influence of reflection of the sensors. $k_e = 0.1$ and $k_o = 0.5$ for weights as Oriola, Vendittelli and Ulivi used in their indoor experiment. Figure 7-78 and Figure 7-80 are well matched with their experiment and indicates Dombi's fuzzy union that is a non-

linear increasing function that accumulates data faster than histogram method. However, this approach also needs multiple detection to distinguish obstacles. In their experiment, ultrasonic sensors were manually placed in known locations and 40 measures were taken.

From Figure 7-81 to Figure 7-84 indicates this approach is more robust with respect to the noise. A membership function is used for the sensor model and the maximum value is not 1.0; for empty membership function is k_e and for occupied membership function is k_o. Therefore, the degree caused by noise is small and the results are improved compared with Bayes's theorem. This approach is suitable in an indoor situation when a vehicle moves less than 0.8 m/s.

For an outdoor environment, Figure 7-89 and Figure 7-97 shows that the laser range scanner with 20% noise is capable when the vehicle moves at 0.83 m/s, but the ultrasonic sensor gives poor performance can not be used.

Nonhomogeneous Markov Chain Approach

The results for nonhomogeneous Markov chain approach are shown from Figure 7-101 to Figure 7-136. The values of weights $m(\cdot)$ are $m(1) = 0.6$, $m(2) = 0.7$, $m(3) = 0.8$, $m(4) = 0.9$, and $m(\geq 5) = 1.0$.

Figure 7-109 to Figure 7-112 shows the map when a sensor has no noise and a vehicle moves on the flat terrain in an outdoor environment. All obstacles and free space are well detected. When the sensor has noise, all obstacle are detected but the degree of certainty becomes lower and there are big holes in free space as seen in from Figure 7-113 to Figure 7-116. There are two ways to improve the quality of the map. One is sensor fusion. By using range data from an ultrasonic sensor and laser range scanner, the degree

of certainty is improved as shown in Figure 7-117 and 7-118. The other is multiple sensing. Figure 7-119 to 7-120 shows the map when the vehicle runs twice around the course. The results show the improvement for the degree of certainty.

When the vehicle changes the pitch angle and roll angle while following the terrain, the sensing sometimes becomes poor and this effect appears in a map. Even though the laser range scanner has no noise and the vehicle moves at 0.83 m/s, this approach can not detect the cylinder #3 in Figure 7-123. Increasing the vehicle speed to 1.5 m/s, this approach can not detect cylinder #3 and cone #7 in Figure 7-125. However, Figure 7-124 and Figure 7-126 show that all obstacles are detected because of the wide angle of the ultrasonic sensor. When the laser range scanner has noise, there is a missing obstacle on the map, and Figure 7-127 and Figure 7-129 show no detection of cone #7. On the other hand, when the ultrasonic sensor has a noise, some false detection occurs. Figure 7-128 shows the map when the vehicle moves at 0.83 m/s and there are twelve false obstacles on the map. When the speed of the vehicle is increased to 1.5 m/s, there are four false obstacles and cylinder #3 is missing on the map. For a small object that is located far from a vehicle, laser range scanner can not detect the object within the sensing field because of the spatial resolution. It decreases the probability of occupancy in an occupied cell and causes the missing object on the map. To improve the quality of the map, sensor fusion is applied. As seen in the case of flat terrain, the degree of certainty is improved but cylinder #3 is still missing as shown Figure 7-131 and 7-132. To detect cylinder #3, multiple sensing is applied. As seen in Figure 7-133 and Figure 7-135, this approach with double detection can detect cylinder #3, even though the laser range scanner has noise. When an ultrasonic sensor is used, there are some false obstacles.

However, because the degree of certainty is emphasized, conventional noise reduction can reduce false obstacles.

Moreover, Figure 7-101 to Figure 7-108 shows that this approach is also suitable for an indoor environment.

Conclusions

This research involved the development of a strategy for map management in a large-scale outdoor environment where data are obtained from a moving vehicle. The management required both obstacle-free space detection and a small size of the map data that are stored by the on-board computer. This section will summarize the author's research and highlight what is unique about it.

The author's map management strategy involved the development of a multi-layered map management system. The system consists of a local grid map and a global contour map. The local grid map deals with obstacle-free space detection using range data from a variety of sensors. The global contour map reduces the size of data from the local grid map. The system maintains the consistency between two maps. The management strategy was implemented and demonstrated in simulation.

The local grid map is represented as a grid model and the management strategy is based on a concept of uncertainty. Uncertainty was classified under one of three categories; randomness, fuzziness, and indeterminacy. From the viewpoint of uncertainty, previous grid model and sensor modeling techniques were discussed in chapter 4 and investigated in chapter 7 for an outdoor environment.

The probability theory approach regards a poor performance of a sensor as randomness and models the sensor by an empty probability density function and an occupied probability density function. To update a grid map, the additive law of probability was applied, assuming a value of a previous map and sensor data are independent from each other. The results obtained in simulation indicate this approach is not suitable for an outdoor environment because of the high sensitivity to noise.

The Bayes's theorem approach also regards poor performance of a sensor as randomness and describes uncertainty by a probabilistic distribution of occupancy. To update a grid map, a probability produced by range data was regarded as a conditional probability and Bayes's theorem was used. The results obtained in simulation shows this approach can be used for an indoor environment but is not suitable for the outdoor environment because of the high sensitivity to noise and less multiple detection.

The histogram method approach regards a poor performance of sensor as randomness as well and implements a simplified sensor model using a histogramic probability distribution. To update a map, the additive law of probability was modified to increase and decrease a cell value by an integer number, assuming a value of a previous map and sensor data are not only independent but also mutually exclusive. The results obtained in simulation indicate this approach requires repeatability of sensing and it is very difficult to use in both indoor and outdoor environments when a vehicle moves more than 0.8 m/s.

The fuzzy logic approach regards noise and poor performance of a sensor as fuzziness and models a sensor by a membership function. To update the map, the fuzzy union operator was used as a non-linear accumulation. The results obtained in simulation

show this approach also requires the repeatability of sensing and it is difficult to use when a vehicle moves faster than 0.8 m/s.

The results obtained for previous grid map techniques conclude that they are not adequate for an outdoor environment. Hence, the author developed a very significant theoretical contribution in this work. He classified uncertainty and described uncertainty of a range sensor caused by noise and poor performance. The real world was modeled using a subset of three elements; obstacle, free space, and sensor noise. A fuzzy model approach was adopted and sensor output was regarded as fuzzy sets. Experimental statistical data are used to assign the degree of membership to a focal element of fuzzy sets and uncertainty was represented in this way. To update a map, a sequence of fuzzy sets was regarded as a stochastic process and a nonhomogeneous Markov chain was applied. The new formula was proved to be strongly ergodic and that the final probability is independent from the vehicle's approach to an obstacle. The results in an outdoor environment support the validity of this work.

The global contour map is represented as a boundary representation. The probabilistic contour was represented by a two dimensional linked list and new conversions between the grid model and boundary representation were developed. A cell in a grid model is regarded as a bubble. Two bubbles are fused and become one bigger bubble verifying the connection between a bubble and a polygon. Forty-seven rules were constructed for fusion rule database. In simulation, the data reduction was achieved while a vehicle moves.

Finally, by integrating a local grid map and a global contour map, the stated goal of this work was achieved in simulation.

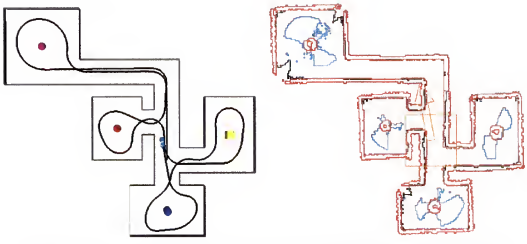

Figure 7-4 Probability Theory (Indoor, Speed 0.83m/s, Laser, No Noise)

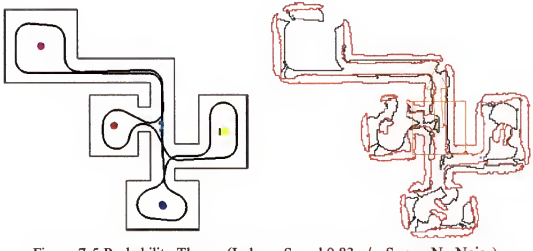

Figure 7-5 Probability Theory (Indoor, Speed 0.83m/s, Sonar, No Noise)

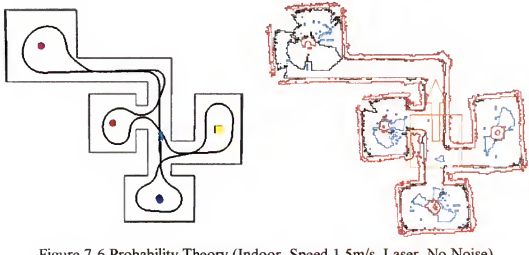

Figure 7-6 Probability Theory (Indoor, Speed 1.5m/s, Laser, No Noise)

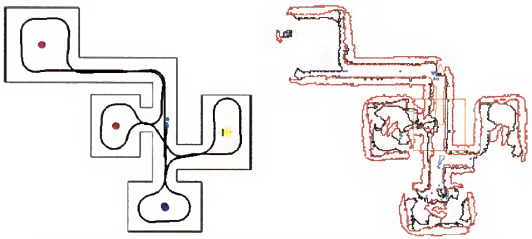

Figure 7-7 Probability Theory (Indoor, Speed 1.5m/s, Sonar, No Noise)

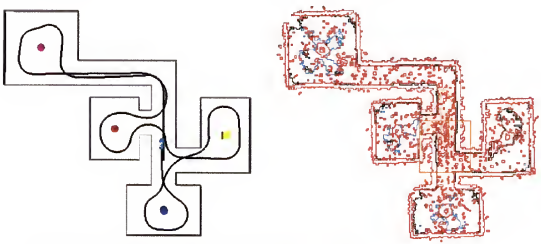

Figure 7-8 Probability Theory (Indoor, Speed 0.83m/s, Laser, 20% Noise)

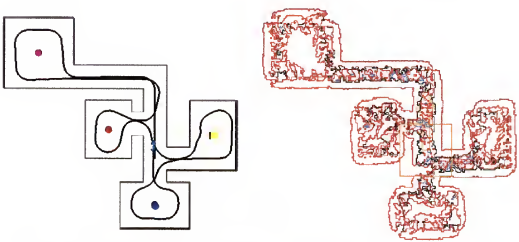

Figure 7-9 Probability Theory (Indoor, Speed 0.83m/s, Sonar, 20% Noise)

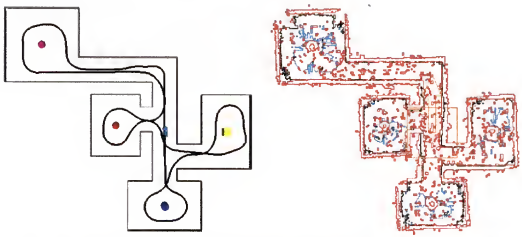

Figure 7-10 Probability Theory (Indoor, Speed 1.5m/s, Laser, 20% Noise)

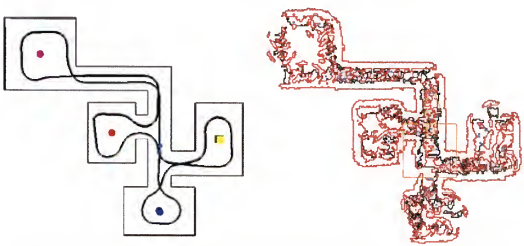

Figure 7-11 Probability Theory (Indoor, Speed 1.5m/s, Sonar, 20% Noise)

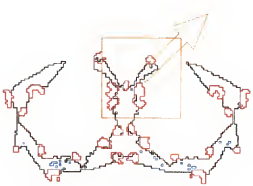

Figure 7-12 Probability Theory
(Flat, Speed 0.83m/s, Laser, No Noise)

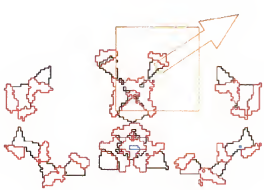

Figure 7-13 Probability Theory
(Flat, Speed 0.83m/s, Sonar, No Noise)

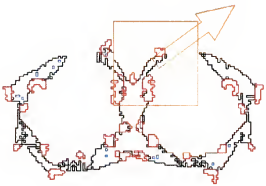

Figure 7-14 Probability Theory
(Flat, Speed 1.5m/s, Laser, No Noise)

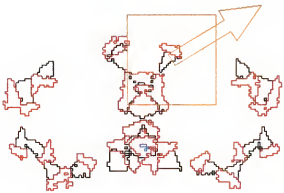

Figure 7-15 Probability Theory
(Flat, Speed 1.5m/s, Sonar, No Noise)

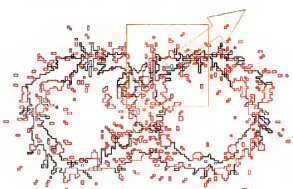

Figure 7-16 Probability Theory
(Flat, Speed 0.83m/s, Laser, 20% Noise)

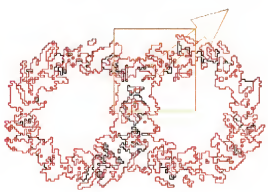

Figure 7-17 Probability Theory
(Flat, Speed 0.83m/s, Sonar, 20% Noise)

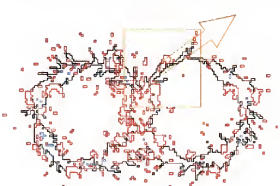

Figure 7-18 Probability Theory
(Flat, Speed 1.5m/s, Laser, 20% Noise)

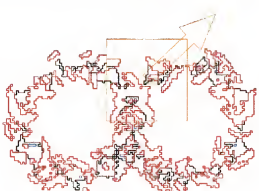

Figure 7-19 Probability Theory
(Flat, Speed 1.5m/s, Sonar, 20% Noise)

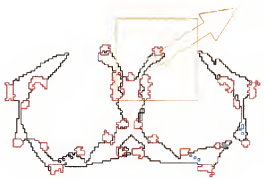

Figure 7-20 Probability Theory (Rugged, Speed 0.83m/s, Laser, No Noise)

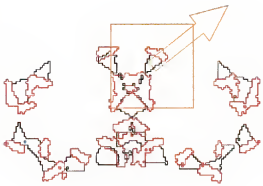

Figure 7-21 Probability Theory (Rugged, Speed 0.83m/s, Sonar, No Noise)

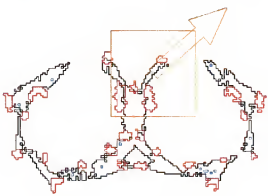

Figure 7-22 Probability Theory (Rugged, Speed 1.5m/s, Laser, No Noise)

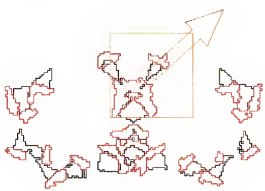

Figure 7-23 Probability Theory (Rugged, Speed 1.5m/s, Sonar, No Noise)

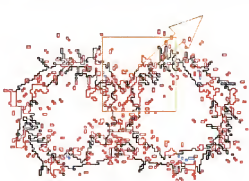

Figure 7-24 Probability Theory (Rugged, Speed 0.83m/s, Laser, 20% Noise)

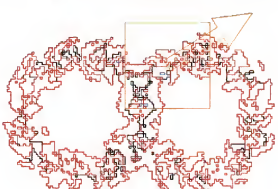

Figure 7-25 Probability Theory (Rugged, Speed 0.83m/s, Sonar, 20% Noise)

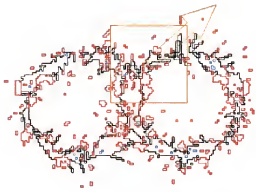

Figure 7-26 Probability Theory (Rugged, Speed 1.5m/s, Laser, 20% Noise)

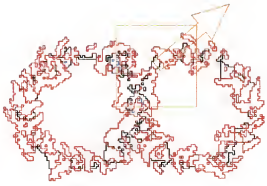

Figure 7-27 Probability Theory (Rugged, Speed 1.5m/s, Sonar, 20% Noise)

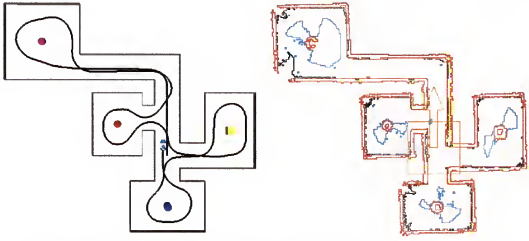

Figure 7-28 Bayes's Theorem (Indoor, Speed 0.83m/s, Laser, No Noise)

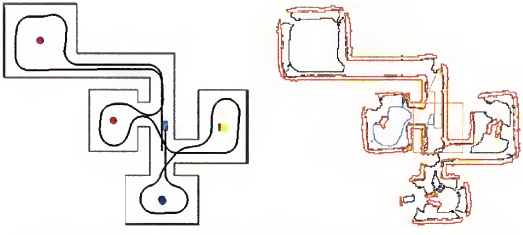

Figure 7-29 Bayes's Theorem (Indoor, Speed 0.83m/s, Sonar, No Noise)

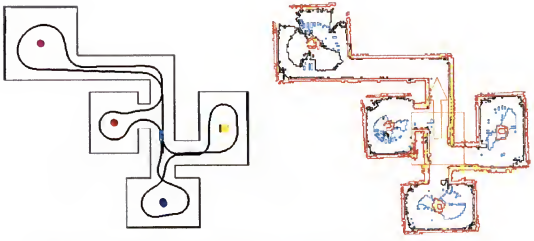

Figure 7-30 Bayes's Theorem (Indoor, Speed 1.5m/s, Laser, No Noise)

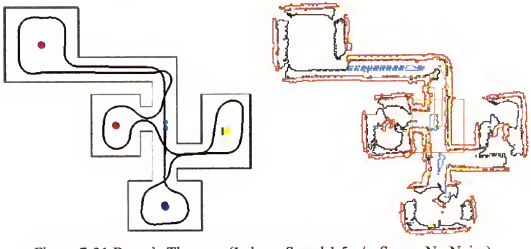

Figure 7-31 Bayes's Theorem (Indoor, Speed 1.5m/s, Sonar, No Noise)

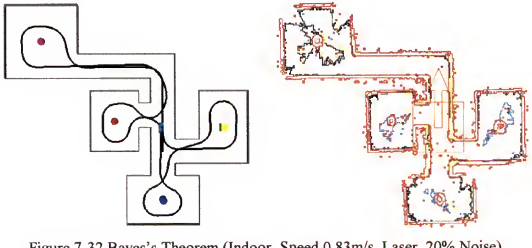

Figure 7-32 Bayes's Theorem (Indoor, Speed 0.83m/s, Laser, 20% Noise)

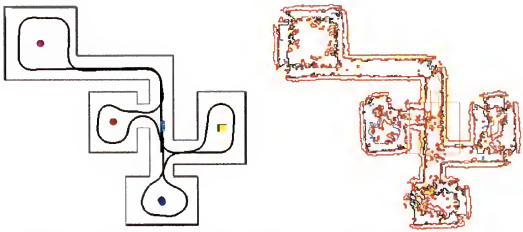

Figure 7-33 Bayes's Theorem (Indoor, Speed 0.83m/s, Sonar, 20% Noise)

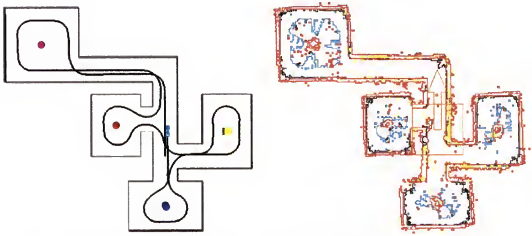

Figure 7-34 Bayes's Theorem (Indoor, Speed 1.5m/s, Laser, 20% Noise)

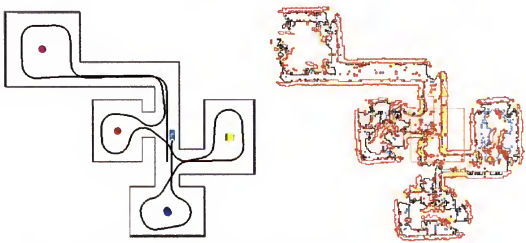

Figure 7-35 Bayes's Theorem (Indoor, Speed 1.5m/s, Sonar, 20% Noise)

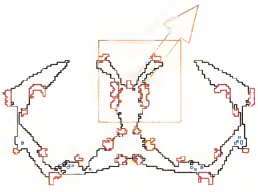

Figure 7-36 Bayes's Theorem
(Flat, Speed 0.83m/s, Laser, No Noise)

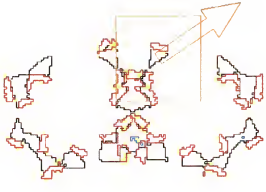

Figure 7-37 Bayes's Theorem
(Flat, Speed 0.83m/s, Sonar, No Noise)

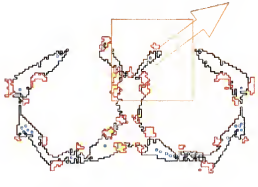

Figure 7-38 Bayes's Theorem
(Flat, Speed 1.5m/s, Laser, No Noise)

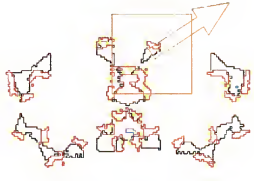

Figure 7-39 Bayes's Theorem
(Flat, Speed 1.5m/s, Sonar, No Noise)

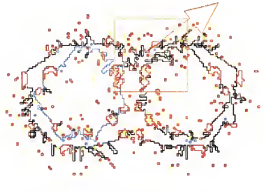

Figure 7-40 Bayes's Theorem
(Flat, Speed 0.83m/s, Laser, 20% Noise)

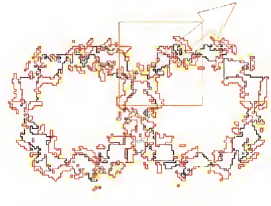

Figure 7-41 Bayes's Theorem
(Flat, Speed 0.83m/s, Sonar, 20% Noise)

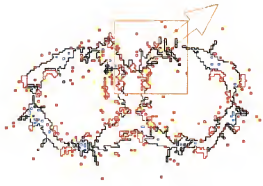

Figure 7-42 Bayes's Theorem
(Flat, Speed 1.5m/s, Laser, 20% Noise)

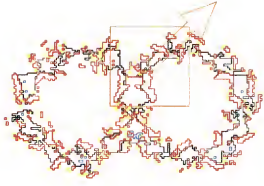

Figure 7-43 Bayes's Theorem
(Flat, Speed 1.5m/s, Sonar, 20% Noise)

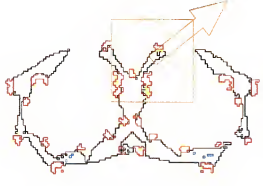

Figure 7-44 Bayes's Theorem
(Rugged, Speed 0.83m/s, Laser, No Noise)

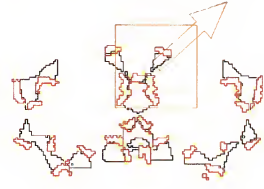

Figure 7-45 Bayes's Theorem
(Rugged, Speed 0.83m/s, Sonar, No Noise)

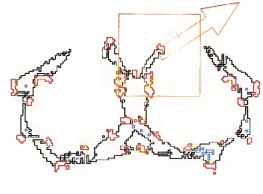

Figure 7-46 Bayes's Theorem
(Rugged, Speed 1.5m/s, Laser, No Noise)

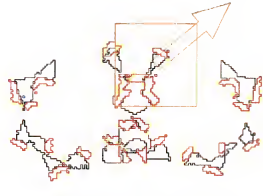

Figure 7-47 Bayes's Theorem
(Rugged, Speed 1.5m/s, Sonar, No Noise)

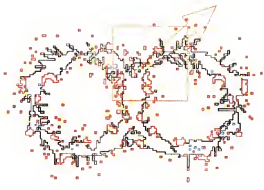

Figure 7-48 Bayes's Theorem (Rugged, Speed 0.83m/s, Laser, 20% Noise)

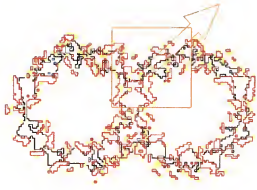

Figure 7-49 Bayes's Theorem (Rugged, Speed 0.83m/s, Sonar, 20% Noise)

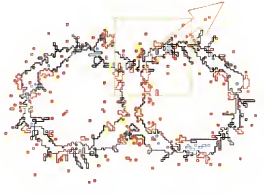

Figure 7-50 Bayes's Theorem (Rugged, Speed 1.5m/s, Laser, 20% Noise)

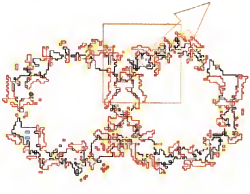

Figure 7-51 Bayes's Theorem (Rugged, Speed 1.5m/s, Sonar, 20% Noise)

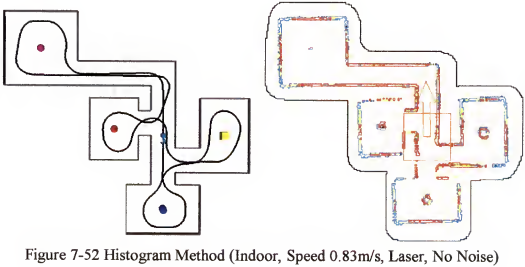

Figure 7-52 Histogram Method (Indoor, Speed 0.83m/s, Laser, No Noise)

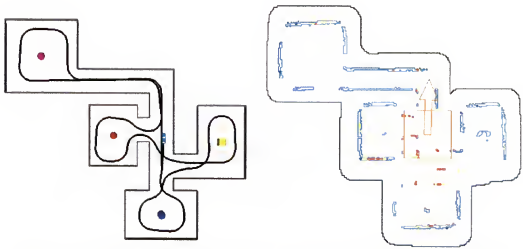

Figure 7-53 Histogram Method (Indoor, Speed 0.83m/s, Sonar, No Noise)

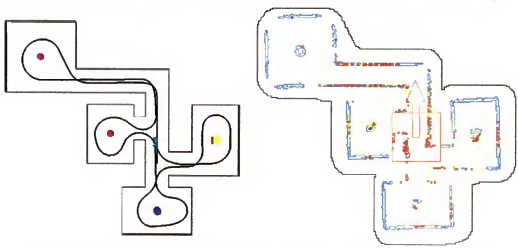

Figure 7-54 Histogram Method (Indoor, Speed 1.5m/s, Laser, No Noise)

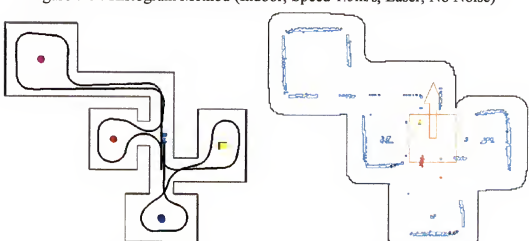

Figure 7-55 Histogram Method (Indoor, Speed 1.5m/s, Sonar, No Noise)

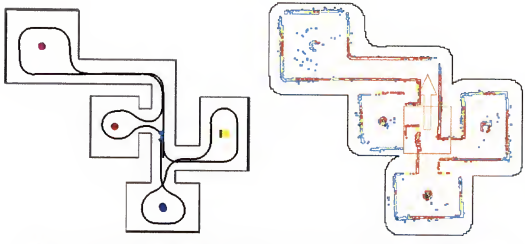

Figure 7-56 Histogram Method (Indoor, Speed 0.83m/s, Laser, 20% Noise)

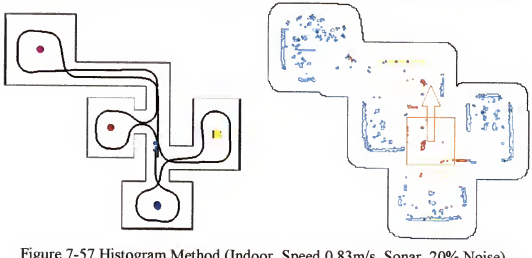

Figure 7-57 Histogram Method (Indoor, Speed 0.83m/s, Sonar, 20% Noise)

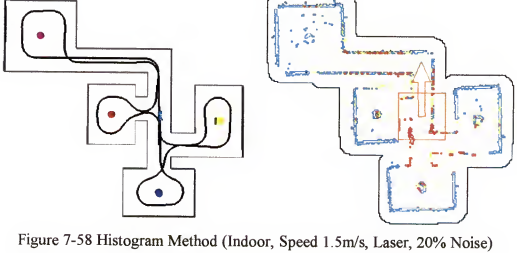

Figure 7-58 Histogram Method (Indoor, Speed 1.5m/s, Laser, 20% Noise)

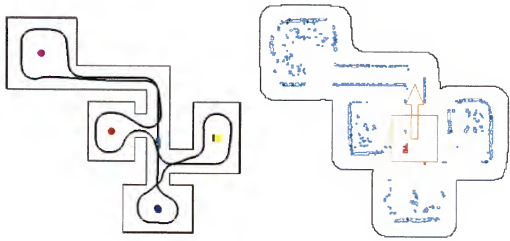

Figure 7-59 Histogram Method (Indoor, Speed 1.5m/s, Sonar, 20% Noise)

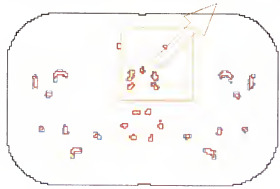

Figure 7-60 Histogram Method
(Flat, Speed 0.42m/s, Laser, No Noise)

Figure 7-61 Histogram Method
(Flat, Speed 0.83m/s, Laser, No Noise)

Figure 7-62 Histogram Method
(Flat, Speed 0.83m/s, Sonar, No Noise)

Figure 7-63 Histogram Method
(Flat, Speed 1.5m/s, Laser, No Noise)

Figure 7-64 Histogram Method
(Flat, Speed 1.5m/s, Sonar, No Noise)

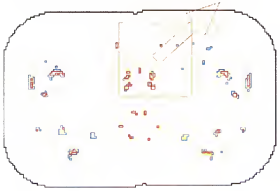

Figure 7-65 Histogram Method
(Flat, Speed 0.83m/s, Laser, 20% Noise)

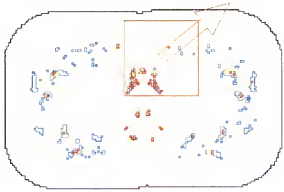

Figure 7-66 Histogram Method
(Flat, Speed 0.83m/s, Sonar, 20% Noise)

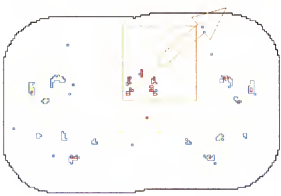

Figure 7-67 Histogram Method
(Flat, Speed 1.5m/s, Laser, 20% Noise)

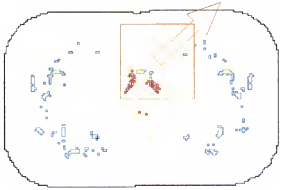

Figure 7-68 Histogram Method
(Flat, Speed 1.5m/s, Sonar, 20% Noise)

Figure 7-69 Histogram Method
(Rugged, Speed 0.83m/s, Laser, No Noise)

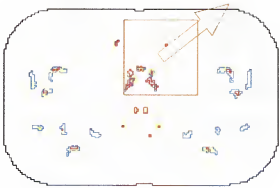

Figure 7-70 Histogram Method
(Rugged, Speed 0.83m/s, Sonar, No Noise)

Figure 7-71 Histogram Method
(Rugged, Speed 1.5m/s, Laser, No Noise)

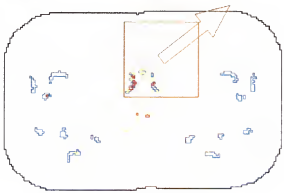

Figure 7-72 Histogram Method
(Rugged, Speed 1.5m/s, Sonar, No Noise)

Figure 7-73 Histogram Method
(Rugged, Speed 0.83m/s, Laser, 20% Noise)

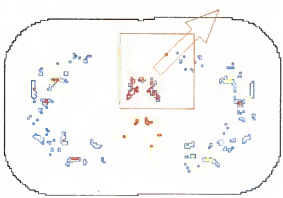

Figure 7-74 Histogram Method
(Rugged, Speed 0.83m/s, Sonar, 20% Noise)

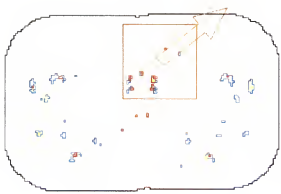

Figure 7-75 Histogram Method (Rugged, Speed 1.5m/s, Laser, 20% Noise)

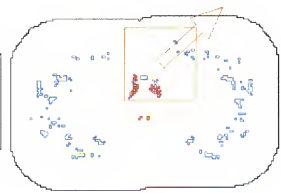

Figure 7-76 Histogram Method (Rugged, Speed 1.5m/s, Sonar, 20% Noise)

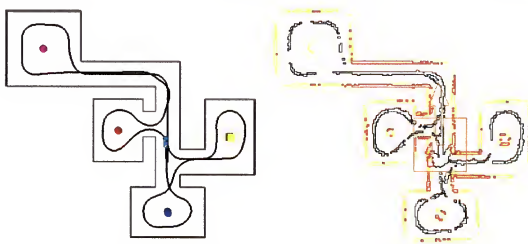

Figure 7-77 Fuzzy Logic (Indoor, Speed 0.83m/s, Laser, No Noise)

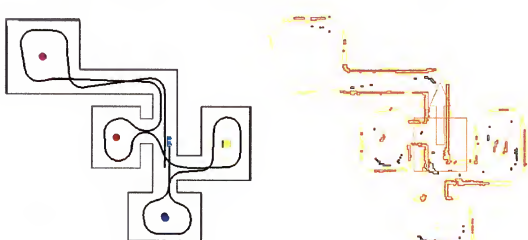

Figure 7-78 Fuzzy Logic (Indoor, Speed 0.83m/s, Sonar, No Noise)

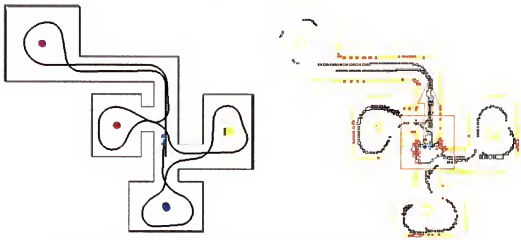

Figure 7-79 Fuzzy Logic (Indoor, Speed 1.5m/s, Laser, No Noise)

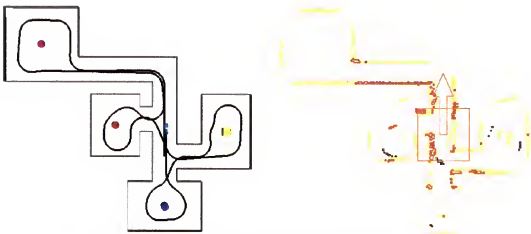

Figure 7-80 Fuzzy Logic (Indoor, Speed 1.5m/s, Sonar, No Noise)

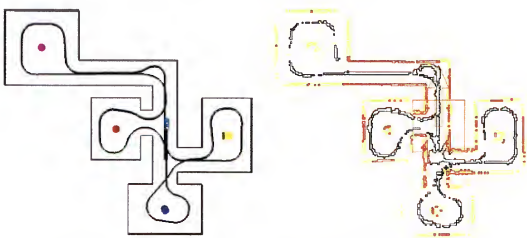

Figure 7-81 Fuzzy Logic (Indoor, Speed 0.83m/s, Laser, 20% Noise)

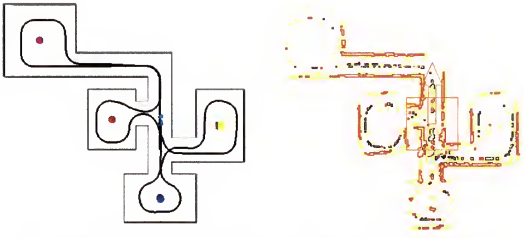

Figure 7-82 Fuzzy Logic (Indoor, Speed 0.83m/s, Sonar, 20% Noise)

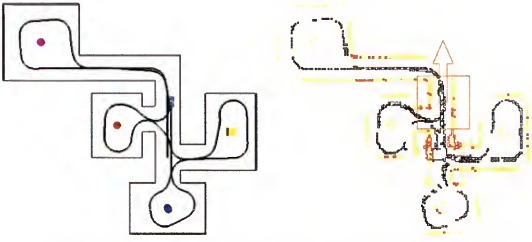

Figure 7-83 Fuzzy Logic (Indoor, Speed 1.5m/s, Laser, 20% Noise)

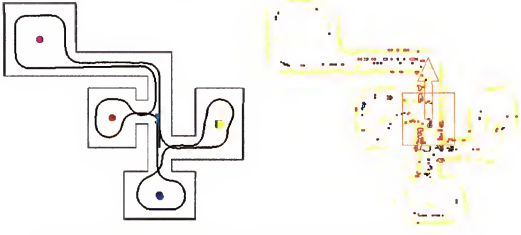

Figure 7-84 Fuzzy Logic (Indoor, Speed 1.5m/s, Sonar, 20% Noise)

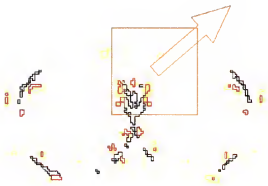

Figure 7-85 Fuzzy Logic
(Flat, Speed 0.83m/s, Laser, No Noise)

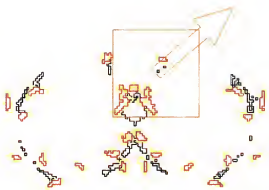

Figure 7-86 Fuzzy Logic
(Flat, Speed 0.83m/s, Sonar, No Noise)

Figure 7-87 Fuzzy Logic
(Flat, Speed 1.5m/s, Laser, No Noise)

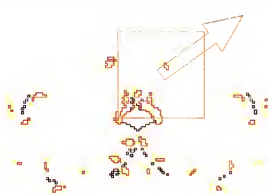

Figure 7-88 Fuzzy Logic
(Flat, Speed 1.5m/s, Sonar, No Noise)

Figure 7-89 Fuzzy Logic
(Flat, Speed 0.83m/s, Laser, 20% Noise)

Figure 7-90 Fuzzy Logic
(Flat, Speed 0.83m/s, Sonar, 20% Noise)

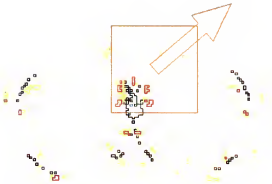

Figure 7-91 Fuzzy Logic
(Flat, Speed 1.5m/s, Laser, 20% Noise)

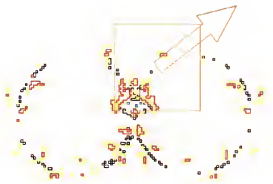

Figure 7-92 Fuzzy Logic
(Flat, Speed 1.5m/s, Sonar, 20% Noise)

Figure 7-93 Fuzzy Logic
(Rugged, Speed 0.83m/s, Laser, No Noise)

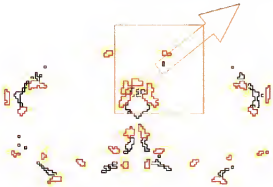

Figure 7-94 Fuzzy Logic
(Rugged, Speed 0.83m/s, Sonar, No Noise)

Figure 7-95 Fuzzy Logic
(Rugged, Speed 1.5m/s, Laser, No Noise)

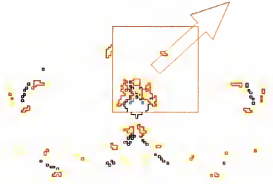

Figure 7-96 Fuzzy Logic
(Rugged, Speed 1.5m/s, Sonar, No Noise)

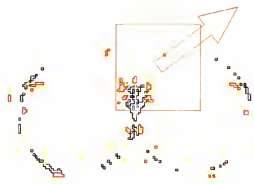

Figure 7-97 Fuzzy Logic
(Rugged, Speed 0.83m/s, Laser, 20% Noise)

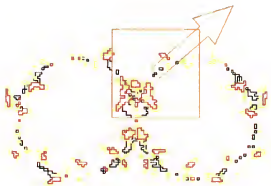

Figure 7-98 Fuzzy Logic
(Rugged, Speed 0.83m/s, Sonar, 20% Noise)

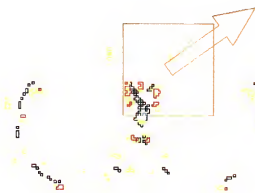

Figure 7-99 Fuzzy Logic
(Rugged, Speed 1.5m/s, Laser, 20% Noise)

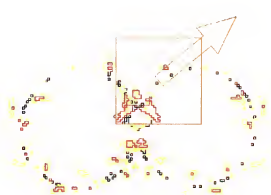

Figure 7-100 Fuzzy Logic
(Rugged, Speed 1.5m/s, Sonar, 20% Noise)

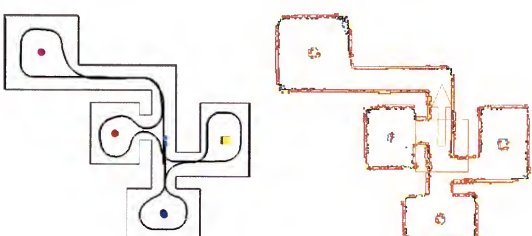

Figure 7-101 Markov Chain (Indoor, Speed 0.83m/s, Laser, No Noise)

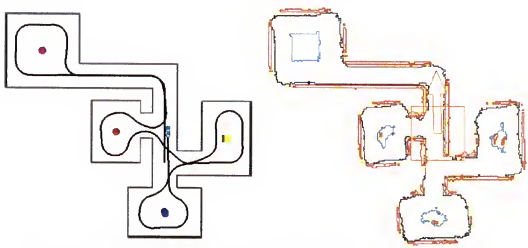

Figure 7-102 Markov Chain (Indoor, Speed 0.83m/s, Sonar, No Noise)

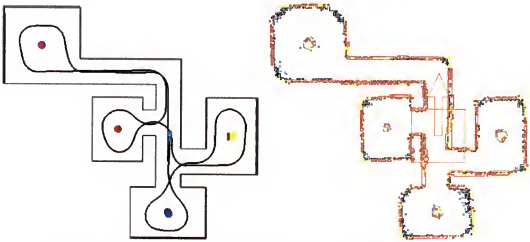

Figure 7-103 Markov Chain (Indoor, Speed 1.5m/s, Laser, No Noise)

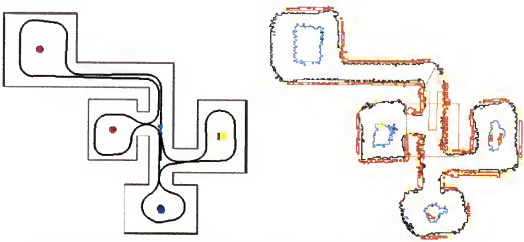

Figure 7-104 Markov Chain (Indoor, Speed 1.5m/s, Sonar, No Noise)

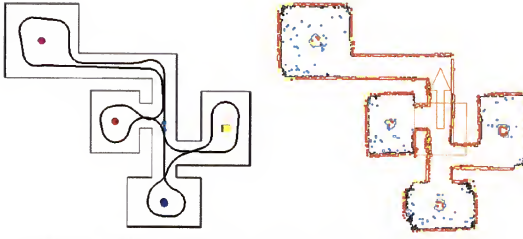

Figure 7-105 Markov Chain (Indoor, Speed 0.83m/s, Laser, 20% Noise)

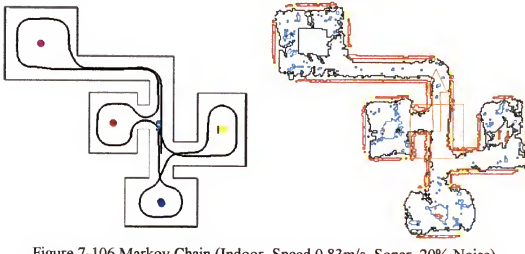

Figure 7-106 Markov Chain (Indoor, Speed 0.83m/s, Sonar, 20% Noise)

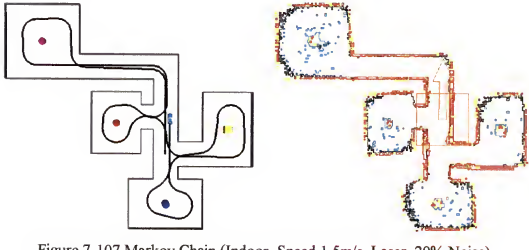

Figure 7-107 Markov Chain (Indoor, Speed 1.5m/s, Laser, 20% Noise)

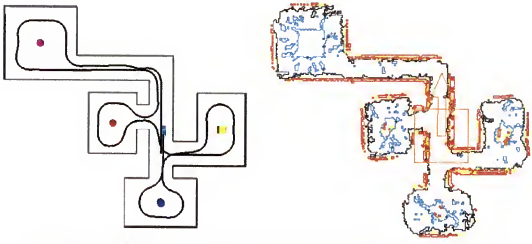

Figure 7-108 Markov Chain (Indoor, Speed 1.5m/s, Sonar, 20% Noise)

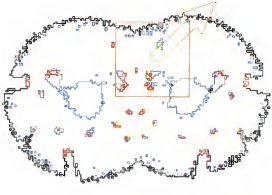

Figure 7-109 Markov Chain
(Flat, Speed 0.83m/s, Laser, No Noise)

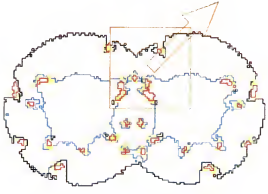

Figure 7-110 Markov Chain
(Flat, Speed 0.83m/s, Sonar, No Noise)

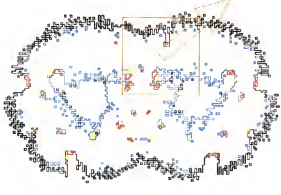

Figure 7-111 Markov Chain
(Flat, Speed 1.5m/s, Laser, No Noise)

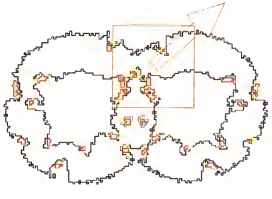

Figure 7-112 Markov Chain
(Flat, Speed 1.5m/s, Sonar, No Noise)

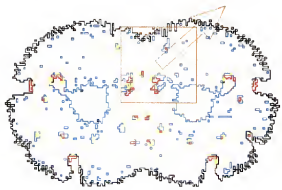

Figure 7-113 Markov Chain
(Flat, Speed 0.83m/s, Laser, 20% Noise)

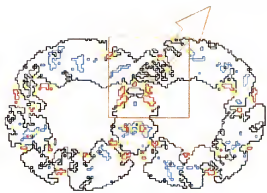

Figure 7-114 Markov Chain
(Flat, Speed 0.83m/s, Sonar, 20% Noise)

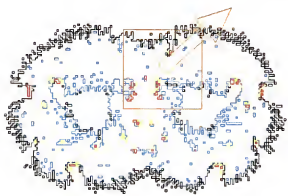

Figure 7-115 Markov Chain
(Flat, Speed 1.5m/s, Laser, 20% Noise)

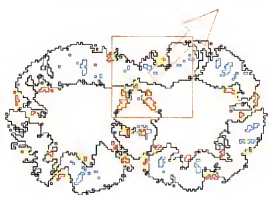

Figure 7-116 Markov Chain
(Flat, Speed 1.5m/s, Sonar, 20% Noise)

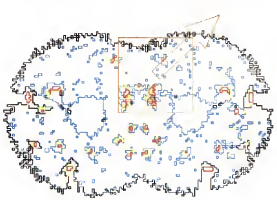

Figure 7-117 Markov Chain
(Flat, Speed 0.83m/s, Fusion, 20% Noise)

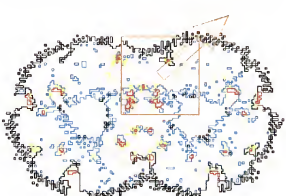

Figure 7-118 Markov Chain
(Flat, Speed 1.5m/s, Fusion, 20% Noise)

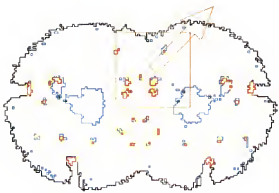

Figure 7-119 Markov Chain
(Flat, 0.83m/s, Laser, 20% Noise, Repeat)

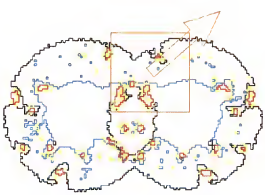

Figure 7-120 Markov Chain
(Flat, 0.83m/s, Sonar, 20% Noise, Repeat)

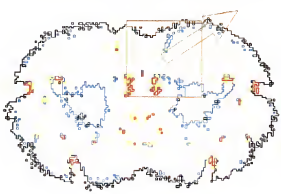

Figure 7-121 Markov Chain
(Flat, 1.5m/s, Laser, 20% Noise, Repeat)

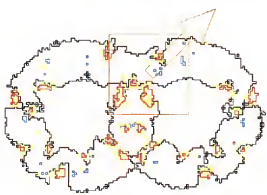

Figure 7-122 Markov Chain
(Flat, 1.5m/s, Sonar, 20% Noise, Repeat)

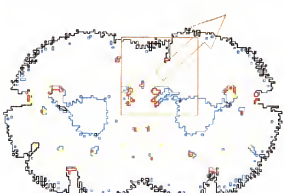

Figure 7-123 Markov Chain
(Rugged, Speed 0.83m/s, Laser, No Noise)

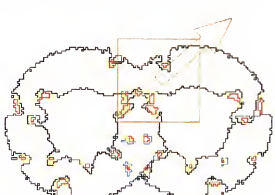

Figure 7-124 Markov Chain
(Rugged, Speed 0.83m/s, Sonar, No Noise)

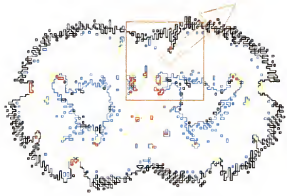

Figure 7-125 Markov Chain
(Rugged, Speed 1.5m/s, Laser, No Noise)

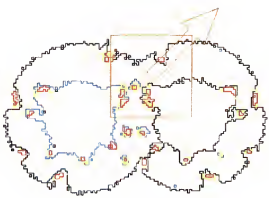

Figure 7-126 Markov Chain
(Rugged, Speed 1.5m/s, Sonar, No Noise)

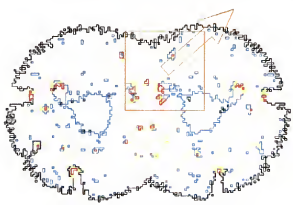

Figure 7-127 Markov Chain
(Rugged, Speed 0.83m/s, Laser, 20% Noise)

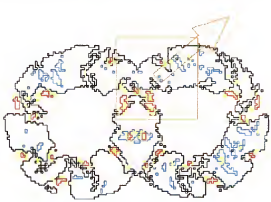

Figure 7-128 Markov Chain
(Rugged, Speed 0.83m/s, Sonar, 20% Noise)

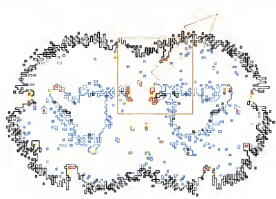

Figure 7-129 Markov Chain
(Rugged, Speed 1.5m/s, Laser, 20% Noise)

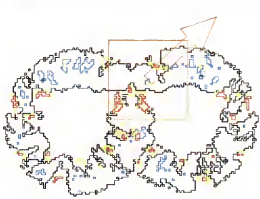

Figure 7-130 Markov Chain
(Rugged, Speed 1.5m/s, Sonar, 20% Noise)

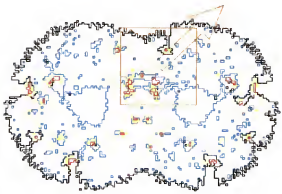

Figure 7-131 Markov Chain (Rugged, Speed 0.83m/s, Fusion, 20%Noise)

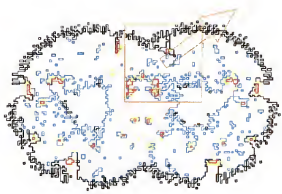

Figure 7-132 Markov Chain (Rugged, Speed 1.5m/s, Fusion, 20%Noise)

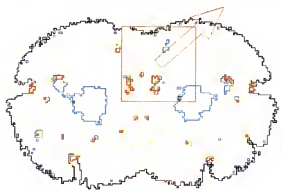

Figure 7-133 Markov Chain (Rugged,0.83m/s,Laser,20%Noise,Repeat)

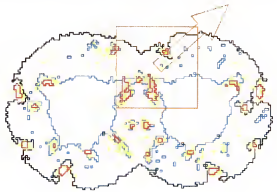

Figure 7-134 Markov Chain (Rugged,0.83m/s,Sonar,20%Noise,Repeat)

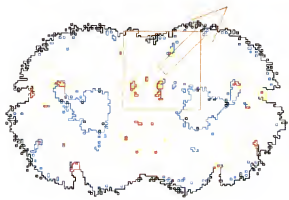

Figure 7-135 Markov Chain (Rugged,1.5m/s,Laser,20%Noise,Repeat)

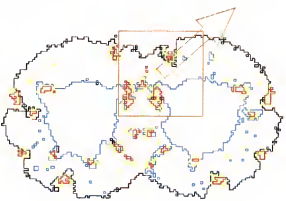

Figure 7-136 Markov Chain (Rugged,1.5m/s,Sonar,20%Noise,Repeat)

APPENDIX
SIX ZONE OBSTACLE DETECTION

Using a vision system developed by the Jet Propulsion Laboratory, a prototype of a six zone obstacle detection method has been developed and tested in an outdoor environment. The vision system consists of two cameras, a Datacube image processing board, a Digi-color frame memory, and a 68040 central processing unit board. Two cameras are installed on a pan tilt devise, are supplied power, and output black and white NTSC video signal. The signals from the left and right cameras are converted to digital data and are stored in the Digi-color frame memory. The central processing unit board, Datacube image processing board and frame memory are connected through a VME bus and all vision processing is done on one 68040 augmented with the Datacube image processing board. In this experiment, the JPL vision system was set to a 54 degree of field of view, 64×60 pixels resolution, and range from 3.0 m to 25 m and calibrated.

Range data from the vision system are contaminated by random noise mainly caused by a wide range of brightness and the complicated nature of objects in an outdoor environment. Therefore, instead of using all range data obtained from the vision system directly, range data are divided into six zones defined in Figure A-1. The closest point of an obstacle in each zone is detected such that (1) it is the closest point in a zone, (2) the height is between 0.9 m and 2.1 m in the vision coordinate system, (3) the distance is between 3.0 m and 25 .0 m, (4) dsum = $\{\Sigma \text{ abs}(d_k - d_0)\}$ / (the number of available

points around d_0). The flowchart is shown in Figure A-2. The detected obstacles in each zone are used by the obstacle avoidance in the same way as ultrasonic sensors which detect the closest point of obstacles within a conical sensing area.

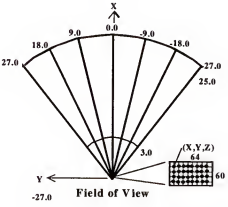

Figure A-1 Definition of Six Zones

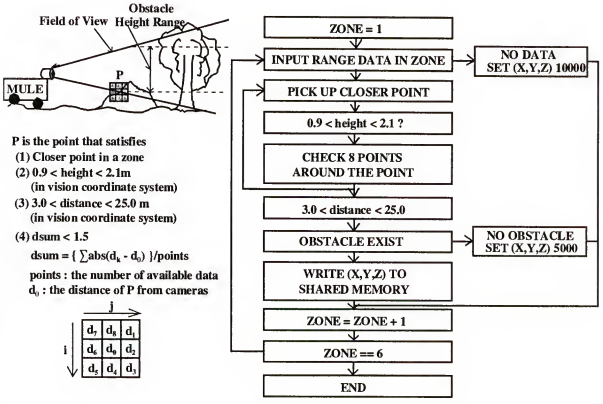

Figure A-2 Algorithm of Six Zone Obstacle Detection

The outdoor testing was conducted in front of Mechanical Building and the vision system data was compared with ultrasonic sensors. The results show that the sampling time is about 1 Hz and the error is within 6 %. The results are summarized in Table A-1, A-2, Figure A-3and A-4. Original in Table A-1 and A-2 indicates the six zone obstacle detection and JPL indicates the usage of function made by JPL.

Table A-1 Sampling Time and Resolution

	ORIGINAL (w/o Image Data)	JPL (w/o Image Data)	ORIGINAL (Image Data)	JPL (Image Data)
64×60 (1 Degree)	1.248673 Hz	1.132320 Hz	1.132075 Hz	1.020643 Hz
128×120 (0.5 Degree)	0.388640 Hz	0.326201 Hz	0.387461 Hz	0.320798 Hz

Table A-2 Detection Accuracy (Static Test)

	TREE		WALL		LADDER		HUMAN		NO OBSTACLE
	5 m	10 m	5 m	10 m	5 m	10 m	5 m	10 m	
SONAR	5.0 m	NO DATA	5.0±0.1 m	NO DATA	NO DATA	NO DATA	4.8±0.1 m	NO DATA	NO DATA
ORIGINAL	5.3±0.1 m	10.0±0.2 m	4.9±0.1 m	9.5 m	5.3±0.3 m	9.4±0.6 m	4.9±0.5 m	9.9±0.2 m	NO DATA
JPL	4.8±0.1 m	10.0±0.2 m	4.9±0.1 m	9.3±0.1 m	5.0±0.1 m	9.8±0.3 m	5.2±0.1 m	10.5±0.4 m	NOISE DATA

Stereo vision system is a passive sensing, longer sensing distance, and higher resolution but slow sampling time. When an obstacle exists in each zone, the six zone obstacle detection method detects an obstacle and return the closest distance in each zone. By regarding the closest distance as range data like a laser range sensor or an ultrasonic sensor, range data from the vision system can be used for a multi-layered map management system. The results show the obtained data from the ultrasonic sensors and stereo vision system are accurate enough for the inputs in an outdoor environment,

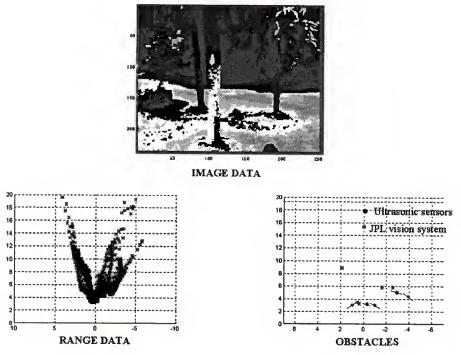

Figure A-3 Obstacle Detection (Tree 3m)

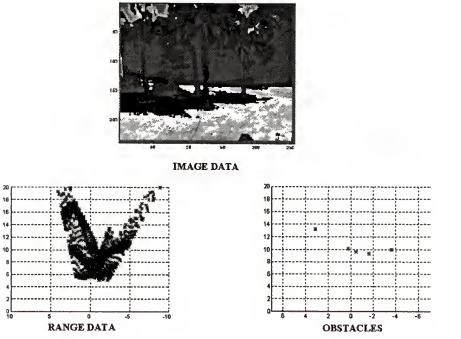

Figure A-4 Obstacle Detection (Tree 8m)

comparing with 10% deviation error of an ultrasonic sensor in the simulation. Therefore, it is expected that an implementation of the map management system would work well in the outdoor environment.

LIST OF REFERENCES

Aya89 Ayache N., O. D. Faugeras, "Maintaining Representations of the Environment of a Mobile Robot," IEEE Transactions on Robotics and Automation, Vol. 5, No. 6, pp 804-819, December 1989.

Bet97 Betke M., L. Gurvits, "Mobile Robot Localization Using Landmarks," IEEE Transaction on Robotics and Automation, Vol. 13, No. 2, pp 251-263, April 1997.

Bor89 Borenstein J., Y. Koren, "Real-time Obstacle Avoidance for Fast Mobile Robots," IEEE Transactions on System, Man, and Cybernetics, Vol. 19, No. 5, pp 1179-1187, September 1989.

Bor91a Borenstein J., Y. Koren, "The Vector Field Histogram-Fast Obstacle Avoidance for Mobile Robots," IEEE Transaction on Robotics and Automation, Vol. 7, No. 3, pp 278-288, June 1991.

Bor91b Borenstein J., Y. Koren, "Histogramic In-Motion Mapping for Mobile Robot Obstacle Avoidance," IEEE Transaction on Robotics and Automation, Vol. 7, No. 4, pp 535-539, August 1991.

Bra92 Brain M., Motif Programming, Digital Press, Newton, MA, 1992.

Bre95 Brezetz S. B., R. Chatila, M. Devy, "Object-based Modeling and Localization in Natural Environments," Proceedings of the IEEE International Conference on Robotics and Automation, Aichi, Japan, pp 2920-2927, 1995.

Bre96 Brezetz S. B., P. Hébert, R. Chatila, M. Devy, "Uncertain Map Making in Natural Environments," Proceedings of the IEEE International Conference on Robotics and Automation, Minneapolis, Minnesota, pp 1048-1053, April 1996.

Bro85 Brooks R. A., "Visual Map Making for a Mobile Robot," Proceedings of the IEEE International Conference on Robotics and Automation, St. Louis, Missouri, pp 824-829, 1985.

Cho90 Cho D. W., "Certainty Grid Representation for Robot Navigation by a Bayesian Method," Robotica, Vol. 8, pp 159-165, 1990.

Dav91 Davis T. E., "Toward an Extrapolation of the Simulated Annealing Convergence Theory onto the Simple Genetic Algorithm," Doctoral Dissertation, University of Florida, 1991.

Del98 Delmotte F., P. Borne, "Modeling of Reliability with Possibility Theory," IEEE Transactions on System, Man, and Cybernetics, Vol. 28, No. 1, pp 78-88, January 1998.

Den96 Deng X., A. Mirzaian, "Competitive Robot Mapping with Homogeneous Markers," IEEE Transactions on Robotics and Automation, Vol. 12, No. 4, pp 532-541, August 1996.

Dub80 Dubois D., H. Prade, Fuzzy Sets and Systems, Academic Press, New York, 1980.

Dub88 Dubois D., H. Prade, Possibility Theory, Plenum Press, New York, 1988.

Dri93 Driankov D., H. Hellendoorn, M. Reinfrank, An Introduction to Fuzzy Control, Spring-Verlag, New York, 1993.

Ekm97 Ekman A., A. Törne, D. Strömberg, "Exploration of Polygonal Environments Using Range Data," IEEE Transaction on System, Man, and Cybernetics, Vol. 27, No. 2, pp 250-255, April 1997.

Elf87a Elfes A., "Sonar-Based Real-World Mapping and Navigation," IEEE Journal of Robotics and Automation, Vol. RA-3, No. 3, pp 249-265, June 1987.

Elf87b Elfes A., L. Matthies, "Sensor Integration for Robot Navigation: Combining Sonar and Stereo Range Data in a Grid-Based Representation," Proceedings of the 26th IEEE Conference on Decision and Control, Los Angeles, CA, pp 1802-1807, December 1987.

Fly88 Flynn A. M., "Combining Sonar and Infrared Sensors for Mobile Robot Navigation," The International Journal of Robotics Research, Vol. 7, No. 6, pp 5-14, December 1988.

Fou93 Foux G., M. Heymann, A. Bruckstein, "Two-dimensional Robot Navigation Among Unknown Stationary Polygonal Obstacles," IEEE Transaction on Robotics and Automation, Vol. 9, No. 1, pp 96-102, February 1993.

Fox97 Fox D., W. Burgard, S. Thrun, "The Dynamic Window Approach to Collision Avoidance," IEEE Robotics and Automation Magazine, Vol. 4, No. 1, pp 23-33, March 1997.

Fuj96 Fujimura K., "Path Planning with Multiple Objectives," IEEE Robotics and Automation Magazine, Vol. 3, No. 1, pp 33-38, March 1996.

Gra95 Grabisch M., "Fuzzy Integral in Multicriteria Decision Making," Fuzzy Sets and Systems 69, pp 279-298, 1995.

Guz97 Guzzoni D., A. Cheyer, L. Julia, K. Konolige, "Many Robots Make Short Work," AI Magazine, pp 55-63, Spring 1997.

Hoe72 Hoel P. G., S. C. Port, C. J. Stone, Introduction to Stochastic Process, Houghton-Mifflin, Boston, 1972.

Hor96 Horst J. A., "Maintaining Multi-level Planar Maps in Intelligent Systems," Proceedings of the IEEE International Conference on Robotics and Automation, Minneapolis, Minnesota, pp 1061-1066, April 1996.

Isa76 Isaacson D. L., R. W. Madsen, Markov Chains Theory and Applications, John Wiley & Sons, New York, 1976.

Kav96 Kavraki L. E., P. Švestka, J. C. Latombe, M. H. Overmars, "Probabilistic Roadmaps for Path Planning in High-Dimensional Configuration Spaces," IEEE Transaction on Robotics and Automation, Vol. 12, No. 4, pp 566-580, August 1996.

Kit96 Kitamura Y., H. Takemura, N. Ahuja, F. Kishino, "Colliding Face Detection among 3-D Objects Using Octree and Polyhedral Shape Representations," Journal of the Robotics Society of Japan, Vol. 14, No. 5, pp 733-742, July 1996.

Kli95 Klir G. J., B. Yuan, Fuzzy Sets and Fuzzy Logic, Prentice Hall PTR, Englewood Cliffs, New Jersey, 1995.

Ko96 Ko J. H., W. J. Kim, M. J. Chung, "A Method of Acoustic Landmark Extraction for Mobile Robot Navigation," IEEE Transactions on Robotics and Automation, Vol. 12, No. 3, pp 478-485, June 1996.

Koc85 Koch E., C. Yeh, G. Hillel, A. Meystel, C. Isik, "Simulation of Path Planning for a System With Vision and Map Updating," Proceedings of the IEEE International Conference on Robotics and Automation, St. Louis, Missouri, pp 146-160, March 1985.

Kri89 Kriegman D. J., E. Triendl, T. O. Binford, "Stereo Vision and Navigation in Buildings for Mobile Robots," IEEE Transaction on Robotics and Automation, Vol. 5, No. 6, pp 792-803, December 1989.

Kui88 Kuipers B. J., T. S. Levitt, "Navigation and Mapping in Large-scale Space," AI Magazine, Vol. 9, No. 2, pp 25-43, Summer 1988.

Kyb96 Kyburg H. E., M. Pittarelli, "Set-Based Bayesianism," IEEE Transaction on System, Man, and Cybernetics, Vol. 26, No. 3, pp 324-339, May 1996.

Lan94 Langer D., J. K. Rosenblatt, M. Hebert, "An Integrated System for Autonomous Off-Road Navigation," Proceedings of the IEEE International Conference on Robotics and Automation, San Diego, CA, pp 414-419, May 1994.

Leo92 Leonard J. J., H. F. Durrant-Whyte, I. J. Cox, "Dynamic Map Building for an Autonomous Mobile Robot," International Journal of Robotics Research, Vol. 11, No. 4, pp 286-298, August 1992.

Leh96 Lehner P. E., K. B. Laskey, D. Dubois, "An Introduction to Issues in Higher Order Uncertainty," IEEE Transaction on System, Man, and Cybernetics, Vol. 26, No. 3, pp 289-292, May 1996.

Lew97 Lewis H. W. III, The Foundations of Fuzzy Control, Plenum Press, New York, 1997.

Lim96 Lim J. H., D. W. Cho, "Multipath Bayesian Map Construction Model from Sonar Data," Robotica, Vol. 14, pp 527-540, 1996.

Liu92 Liu Y., S. Arimoto, "Path Planning Using a Tangent Graph for Mobile Robots Among Polygonal and Curved Obstacles," International Journal of Robotics Research, Vol. 11, No. 4, pp 376-382, August 1992.

Liu95 Liu Y., S. Arimoto, "Finding the Shortest Path of a Disc Among Polygonal Obstacles Using a Radius-Independent Graph," IEEE Transactions on Robotics and Automation, Vol. 11, No. 5, pp 682-691, October 1995.

Mat95 Matthies L., A. Kelly, T. Litwin, "Obstacle Detection for Unmanned Ground Vehicles: A Progress Report," Jet Propulsion Laboratory, pp 1-15, April 1995.

Mor85 Moravec H. P., A. Elfes, "High Resolution Maps from Wide Angle Sonar," Proceedings of the IEEE International Conference on Robotics and Automation, St. Louis, Missouri, pp 116-121, 1985.

Mor88 Moravec H. P., "Sensor Fusion in Certainty Grids for Mobile Robots," AI Magazine, pp 61-74, Summer 1988.

Mur97 Murray D., C. Jennings, "Stereo Vision Based Mapping and Navigation for Mobile Robots," Proceedings of the IEEE International Conference on Robotics and Automation, Albuquerque, NM, pp 1694-1699, April 1997.

Mur98 Murphy R. R., "Dempster-Shafer Theory for Sensor Fusion in Autonomous Mobile Robots," IEEE Transactions on Robotics and Automation, Vol. 14, No. 2, pp 197-206, April 1998.

Nea96 Neapolitan R. E., "Is Higher-Order Uncertainty Needed?," IEEE Transactions on System, Man, and Cybernetics, Vol. 26, No. 3, pp 294-302, May 1996.

Ngu95 Nguyen H. T., M. Sugeno, R. Tong, R. R. Yager, Theoretical Aspects of Fuzzy Control, John Wiley & Sons Inc, New York, 1995.

Ori95 Oriolo G., M. Vendittelli, G. Ulivi, "On-line Map Building and Navigation for Autonomous Mobile Robots," Proceedings of the IEEE International Conference on Robotics and Automation, Aichi, Japan, pp 2900-2906, June 1995.

Ori97 Oriolo G., G. Ulivi, M. Vendittelli, "Fuzzy Maps: A New Tool for Mobile Robot Perception and Planning," Journal of Robotic Systems, Vol. 14, No. 3, pp 179-197, March 1997.

Ori98 Oriolo G., G. Ulivi, M. Vendittelli, "Real-time Map Building and Navigation for Autonomous Robots in Unknown Environments," IEEE Transactions on System, Man, and Cybernetics, Vol. 28, No. 3, pp 316-333, June 1998.

Osu96 Osuna R. G., R. C. Luo, "LOLA: Probabilistic Navigation for Topological Maps," AI Magazine, Vol. 17, No. 1, pp 55-62, Spring 1996.

Pag98 Pagac D., E. M. Nebot, H. D. Whyte, "An Evidential Approach to Map-Building for Autonomous Vehicles," IEEE Transactions on Robotics and Automation, Vol. 14, No. 4, pp 623-629, August 1998.

Par62 Parzen E., Stochastic Process, Holden-Day Inc., New York, 1962.

Pip97 Pipe A. G., B. Carse, A. Winfield, "A Topological Map Based Navigation System for Mobile Robotics," Proceedings of the International Conference on System, Man, and Cybernetics, Orlando, FL, pp 4394-4399, October 1997.

Ple94 Pletta J. B., "Autonomous Navigation for Structured Exterior Environments," Proceedings of ASCE Specialty Conference on Robotics for Challenging Environments, Albuquerque, NM, pp 79-87, February 1994.

Pol95 Poloni M., G. Ulivi, M. Vendittelli, "Fuzzy Logic and Autonomous Vehicles: Experiments in Ultrasonic Vision," Fuzzy Sets and Systems 69, pp 15-27, 1995.

Qia95 Qiao L., M. Sato, H. Takeda, "Learning Algorithm of Environmental Recognition in Driving Vehicle," IEEE Transactions on System, Man and Cybernetics, Vol. 25, No. 6, pp 917-925, June 1995.

Ral96 Ralescu D. A., M. Sugeno, "Fuzzy Integral Representation," Fuzzy Sets and Systems 84, pp 127-133, 1996.

Ran93 Rankin A. L., "Path Planning and Path Execution Software for an Autonomous Non-Holonomic Robot Vehicle," Master's Thesis, University of Florida, 1993.

Ran94 Rankin A. L., D. G. Armstrong II, C. D. Crane III, "Navigation of an Autonomous Robot Vehicle," Proceedings of ASCE Specialty Conference on Robotics for Challenging Environments, Albuquerque, NM, pp 44-51, February 1994.

Ran97 Rankin A. L., "Development of Path Tracking Software for an Autonomous Steered-wheeled Robotic Vehicle and its Trailer," Doctoral Dissertation, University of Florida, 1997.

Rao95 Rao N. S. V., "Robot Navigation in Unknown Generalized Polygonal Terrains Using Vision Sensors," IEEE Transactions on System, Man, and Cybernetics, Vol. 25, No. 6, pp 947-961, June 1995.

Ras90 Raschke U., J. Borenstein, "A Comparison of Grid-type Map-building Techniques by Index of Performance," Proceedings of the IEEE International Conference on Robotics and Automation, Cincinnati, Ohio, pp 1828-1832, May 1990.

Ren93 Rencken W. D., "Concurrent Localisation and Map Building for Mobile Robots Using Ultrasonic Sensors," Proceedings of the IEEE/RSJ International Conference on Intelligent Robots and Systems, Yokohama, Japan, pp 2192-2197, July 1993.

San96 Santos V., J. G. M. Gonçalves, F. Vaz, "Local Perception Maps for Autonomous Robot Navigation," Proceedings of the IEEE/RSJ International Conference on Intelligent Robots and Systems, Osaka, Japan, pp 821-827, 1996.

Sim96 Simsarian K. T., T. J. Olson, N. Nandhakumar, "View-Invariant Regions and Mobile Robot Self-Localization," IEEE Transactions on Robotics and Automation, Vol. 12, No. 5, pp 810-816, October 1996.

Sme81 Smets P., "The Degree of Belief in a Fuzzy Event", Information Science 25, pp 1-19, 1981.

Ste95 Stein F., Medioni G., "Map-Based Localization Using the Panoramic Horizon," IEEE Transactions on Robotics and Automation, Vol. 11, No. 6, pp 892-896, December 1995.

Stu94 Stuck E. R., A. Manz, D. A. Green, S. Elgazzar, "Map Updating and Path Planning for Real-time Mobile Robot Navigation," National Research Council of Canada, NRC No. 37132, pp 753-760, 1994.

Tak95 Takizawa H., Y. Shirai, J. Miura, "Selective Refinement of 3-D Scene Description by Attentive Observation for Mobile Robot," Journal of the Robotics Society of Japan, Vol. 13, No. 7, pp 963-970, October 1995.

Tal96 Talluri R., J. K. Aggarwal, "Mobile Robot Self-Location Using Model-Image Feature Correspondence," IEEE Transactions on Robotics and Automation, Vol. 12, No. 1, pp 63-77, February 1996.

Wac95 Wackerly D. D., W. Mendenhall III, R. L. Scheaffer, Mathematical Statistics with Applications, Duxbury Press, Boston, 1995.

Wal95 Wallner F., R. Graf, R. Dillmann, "Real-time Map Refinement by Fusing Sonar and Active Stereo-Vision," Proceedings of the IEEE International Conference on Robotics and Automation, Aichi, Japan, pp 2968-2973, June 1995.

Wan92 Wang Z., G. Klir, Fuzzy Measure Theory, Plenum Press, New York, 1992.

Wer94 Wernecke J., The Inventor Mentor, Addison-Wesley Publishing Company, Reading, MA, 1994.

Woo94 Woodfill J., R. Zabih, O. Khatib, "Real-time Motion Vision for Robot Control in Unstructured Environments," Proceedings of ASCE Specialty Conference on Robotics for Challenging Environments, Albuquerque, NM, pp 10-18, February 1994.

Yag95 Yagi Y., Y. Nishizawa, M. Yachida, "Map-Based Navigation for a Mobile Robot with Omnidirectional Image Sensor COPIS," IEEE Transactions on Robotics and Automation, Vol. 11, No. 5, pp 634-647, October 1995.

Yan97 Yang C. C., "Fuzzy Bayesian Inference," Proceedings of the International Conference on System, Man, and Cybernetics, Orlando, FL, pp 2707-2712, October 1997.

Zad86 Zadeh L. A., "A Simple View of the Dempster-Shafer Theory of Evidence and its Implication for the Rule of Combination," AI Magazine, pp 85-90, Summer 1986.

Zha92a Zhang Z., O. Faugeras, "A 3D World Model Builder with a Mobile Robot," International Journal of Robotics Research, Vol. 11, No. 4, pp 269-285, August 1992.

Zha92b Zhang Y., R. E. Webber, "On Combining the Hough Transform and Occupancy Grid Methods for Detection of Moving Objects," Proceedings of the IEEE/RSJ International Conference on Intelligent Robots and Systems, Raleigh, North Carolina, pp 2155-2160, July 1992.

Zha96 Zhang Y., R. E. Webber, "Dynamic World Modeling for a Mobile Robot among Moving Objects," Robotica, Vol. 14, part 5, pp 553-560, 1996.

BIOGRAPHICAL SKETCH

Takao Okui enrolled at Nagoya University in Japan in April 1984, and was awarded the degree of Bachelor of Science in Electronic and Mechanical Engineering in March 1988 and the degree of Master of Science in Electronic and Mechanical Engineering in March 1990.

In April 1990, he started to work in the Technical Research and Development Institute as a researcher. However, he decided to work upon completion of a doctoral degree in mechanical engineering.

In August 1995, Takao was admitted to the Graduate School of the University of Florida. In March 1996, he was rewarded for academic achievement by Office of International Studies and Program, and also presidential recognition by the University of Florida in April 1996. In April 1997, he was recognized for outstanding academic achievement by College of Engineering.

I certify that I have read this study and that in my opinion it conforms to acceptable standards of scholarly presentation and is fully adequate, in scope and quality, as a dissertation for the degree of Doctor of Philosophy.

Carl D. Crane III, Chairman
Professor of Mechanical Engineering

I certify that I have read this study and that in my opinion it conforms to acceptable standards of scholarly presentation and is fully adequate, in scope and quality, as a dissertation for the degree of Doctor of Philosophy.

Joseph Duffy
Graduate Research Professor of
Mechanical Engineering

I certify that I have read this study and that in my opinion it conforms to acceptable standards of scholarly presentation and is fully adequate, in scope and quality, as a dissertation for the degree of Doctor of Philosophy.

John Ziegert
Associate Professor of
Mechanical Engineering

I certify that I have read this study and that in my opinion it conforms to acceptable standards of scholarly presentation and is fully adequate, in scope and quality, as a dissertation for the degree of Doctor of Philosophy.

Paul Mason
Assistant Professor of
Mechanical Engineering

I certify that I have read this study and that in my opinion it conforms to acceptable standards of scholarly presentation and is fully adequate, in scope and quality, as a dissertation for the degree of Doctor of Philosophy.

Murali Rao
Professor of Mathematics

This dissertation was submitted to the Graduate Faculty of the College of Engineering and to the Graduate School and was accepted as partial fulfillment of the requirements for the degree of Doctor of Philosophy.

May 1999

Winfred M. Phillips
Dean, College of Engineering

M. J. Ohanian
Dean, Graduate School